EUROPEAN JOURNAL OF PURE AND APPLIED MATHEMATICS
2026, Vol. 19, Issue 2, Article Number 7298
ISSN 1307-5543 – ejpam.com
Published by New York Business Global

A New Crossover Monkeypox Disease Mathematical Model Based on Fractal Fractional Caputo-Katugampola Derivative: Numerical Solutions

Seham M. Al-Mekhlafi[1,2,*], Ahmed Boudaoui[3], Noura Laksaci[3], Thabet Abdeljawad[4,5,6], Hisham M. Alkhawar[7]

[1] *Department of Mathematics, Sana'a University, Sana'a, Yemen*
[2] *Jadara University Research Center, Jadara University, Irbid, Jordan*
[3] *Laboratory of Mathematics Modeling and Applications, University of Adrar, Adrar, Algeria*
[4] *Department of Mathematics and Sciences, Prince Sultan University, Riyadh 11586, Saudi Arabia*
[5] *Department of Fundamental Sciences, Faculty of Engineering and Architecture, Istanbul Gelisim University, Avcılar, Istanbul 34310, Türkiye*
[6] *Department of Mathematics and Applied Mathematics, Sefako Makgatho Health Sciences University, Garankuwa, Medusa 0204, South Africa*
[7] *Preparatory Year Program, Computer Department, Prince Sultan University, Riyadh 11586, Saudi Arabia*

Abstract. Following the 2022 multi-country outbreak, monkeypox has emerged as a major global health concern. However, existing models inadequately capture the memory effects, randomness, and cross-species dynamics characteristic of its transmission. This study addresses this gap by developing a novel hybrid epidemiological model that integrates, for the first time, fractal-fractional Caputo-Katugampola derivatives with fractional Brownian motion. The framework uniquely combines a deterministic phase encoding long-term memory with a stochastic phase capturing environmental fluctuations. Using Perov's fixed-point theorem, we prove solution existence and uniqueness, then develop two numerical schemes: a κ-nonstandard finite difference method and an adapted Euler-Maruyama method. Sensitivity and bifurcation analyses reveal that transmission-related parameters are the primary drivers of disease dynamics, leading to the emergence of a forward bifurcation that marks the transition from disease-free to endemic states. Numerical simulations, calibrated with real outbreak data from the United States, demonstrate excellent agreement and highlight the critical role of memory and stochasticity in shaping infection trajectories. The results underscore the utility of fractal-fractional stochastic modeling for improving predictive power and informing targeted intervention strategies in emerging epidemics.

2020 Mathematics Subject Classifications: 34A08, 60G22, 60H10, 92D30, 65L12, 47H10
Key Words and Phrases: Fractal–fractional derivatives, epidemiological modeling of monkeypox, κ-nonstandard discretization scheme, adapted Euler–Maruyama method for stochastic systems

*Corresponding Author.
DOI: https://doi.org/10.29020/nybg.ejpam.v19i2.7298

Email addresses: sih.almikhlafi@su.edu.ye (S. M. Al-Mekhlafi), ahmedboudaoui@univ-adrar.edu.dz (A. Boudaoui), nor.laksaci@univ-adrar.edu.dz (N. Laksaci), tabdeljawad@psu.edu.sa (T. Abdeljawad), halkhawar@psu.edu.sa (H. M. Alkhawar)

1. Introduction

In recent decades, the emergence and global spread of zoonotic diseases have underscored the urgent need for robust predictive models to support public health responses. One such re-emerging pathogen is the monkeypox virus (Mpox), a zoonotic Orthopoxvirus that can be transmitted from animals to humans and between humans. The disease has drawn significant global attention due to its rapid cross-border spread, lack of widely available vaccines or targeted treatments, and the potential for high morbidity and mortality rates in affected populations. While monkeypox was historically endemic in parts of Central and West Africa, the 2022 outbreak revealed the virus's capacity for sustained human-to-human transmission in non-endemic regions, posing a serious global health threat [1–4].

On the other hand, there are various tools utilized before setting effective preventive control interventions. Mathematical modeling plays a critical role in understanding and predicting the spread of infectious diseases [5]. Classical compartmental models have been instrumental in providing insight into the dynamics of epidemics and guiding intervention strategies. However, these models often fall short in capturing the inherent complexity of biological systems, particularly when dealing with memory effects, environmental variability, and nonlocal interactions. To overcome these limitations, researchers have increasingly turned to fractional-order models, which offer a natural framework to incorporate memory and hereditary properties of biological systems through non-integer order derivatives [6–8].

The complexity of modeling natural processes that exhibit crossover behaviors has motivated the development of a new class of derivatives based on piecewise operators, first introduced by Atangana et al. [9]. These operators have since been applied to a variety of epidemiological contexts: Atangana et al. [10] employed them to capture abrupt changes in disease transmission under varying intervention policies; Alalhareth et al. [11] developed numerical schemes tailored to piecewise fractional models for realistic epidemic data fitting; Atangana and Owolabi [12] analyzed crossover dynamics in co-infection scenarios with memory effects; Sweilam et al. [13] applied the framework to describe stochastic–deterministic transitions in infectious disease spread; Shah et al. [14] investigated variable-order formulations for complex disease pathways; and Wu et al. [15] extended the approach to multi-scale population systems. Collectively, these studies highlight the flexibility and effectiveness of piecewise operators in capturing complex temporal dynamics, thereby motivating their adoption in the present monkeypox modeling framework.

Recent advancements in fractional calculus have significantly enhanced the modeling of complex biological systems by incorporating memory, heredity, and non-local interactions [16, 17]. In particular, the development of crossover models, which combine distinct dynamic regimes such as deterministic and stochastic phases or variable-order operators, has proven highly effective in capturing the real-world progression of diseases like diabetes [18–20]. For instance, novel frameworks have been developed to analyze the dynamics of diabetes using time-delay variable-order models [18] and crossover fractal-fractional stochastic formulations [19], with further extensions to optimal control strategies [20]. Additionally, efficient numerical methods for fractional partial differential equations involving the Ψ-Caputo derivative have been successfully applied to cancer tumor modeling [21]. These methodological innovations provide the rigorous foundation upon which we develop our proposed hybrid model for monkeypox transmission dynamics. Moreover,

recent works have demonstrated the utility of crossover modeling frameworks that combine deterministic and stochastic regimes with varying memory effects to simulate real-world biological systems. For example, crossover models for cholera dynamics [22] and cancer-immune interactions [23] have successfully incorporated both singular and nonsingular fractional kernels or variable-order formulations to capture complex transitions in behavior. These studies highlight the effectiveness of hybrid models in bridging short-term randomness with long-term memory, providing deeper insight into the progression and control of infectious and chronic diseases.

Very recently, a generalized Caputo-Katugampola ($C\kappa$) derivative was proposed in [24, 25] by Katugampola, and further he proved the existence of solutions of $C\kappa$ fractional differential equations in [26]. This type of derivative generalizes two familiar fractional derivatives, namely, Caputo and the Hadamard fractional derivatives to a single form.

Building on this foundation, recent advances have introduced *fractal-fractional derivatives*, which combine fractional dynamics with fractal structures to better reflect irregular and scale-invariant processes observed in real-world epidemics. Among these, the *Caputo-Katugampola fractional derivative* has emerged as a powerful and flexible tool that generalizes classical Caputo and Hadamard derivatives, allowing for more accurate modeling of complex biological and physical systems. Moreover, the use of *stochastic modeling*, particularly with fractional Brownian motion, provides a rigorous way to account for random fluctuations, heterogeneous contact patterns, and uncertainty in disease transmission dynamics [13, 23]. The use of the fractal-fractional Caputo–Katugampola derivative is motivated by its ability to simultaneously capture long-term memory, heterogeneous temporal scaling, and fractal-like transmission patterns that arise in zoonotic epidemics. Moreover, the piecewise deterministic–stochastic formulation reflects the existence of distinct epidemic regimes: a structured deterministic phase dominated by biological mechanisms, and a later stochastic phase influenced by environmental uncertainty and random contact fluctuations. This hybrid framework therefore provides a biologically realistic and mathematically flexible representation of monkeypox dynamics.

The main objective of this article is to develop and analyze a novel crossover epidemiological model for monkeypox transmission by integrating fractal-fractional calculus with stochastic processes. The model captures complex epidemic behavior by transitioning between two regimes: a deterministic phase governed by the fractal-fractional Caputo-Katugampola derivative, and a stochastic phase driven by fractional Brownian motion (FBM). This hybrid formulation enables the incorporation of both long-term memory effects and random environmental fluctuations, which are essential to realistically simulate emerging zoonotic diseases. To analyze the model, we establish the existence and uniqueness of solutions using fixed point theory in generalized Banach spaces, and implement a combination of a κ-nonstandard finite difference method (κ-NFDM) and adapted or nonstandard modified Euler–Maruyama method (NMEMM) to numerically solve the system. We further perform bifurcation analysis to identify threshold dynamics driven by key transmission parameters, and conduct sensitivity analysis to determine which biological factors most strongly influence the number of infected individuals. The model is validated against real monkeypox outbreak data from the United States, demonstrating high predictive accuracy. Overall, the study provides a biologically grounded and mathematically rigorous framework for understanding monkeypox dynamics and supporting effective public health intervention strategies.

The remainder of this paper is organized as follows. In Section 2, we present the formulation

of the crossover monkeypox model, integrating the deterministic fractal-fractional and stochastic regimes. Section 3 is devoted to a qualitative analysis of the deterministic system, including positivity, boundedness, sensitivity analysis results, and a detailed bifurcation analysis to explore threshold behavior. In Section 4, we investigate the existence and uniqueness of solutions to the fractal-fractional system using fixed point theory within a generalized Banach space and the stochastic system. Section 5 describes the construction of numerical schemes, including a κ-nonstandard finite difference method for the deterministic phase and a nonstandard modified modified Euler–Maruyama method for the stochastic phase. Section 6 presents comprehensive numerical simulations calibrated with real outbreak data, demonstrating the model's accuracy and dynamic behavior under varying parameter values. The results highlight the impact of key epidemiological factors and identify the most influential biological parameters governing disease transmission. Finally, Section 7 concludes the paper with a summary of key findings and directions for future research.

2. Notations and Preliminaries

We review some key definitions of fractional calculus in this section, which are used in the subsequent portions of the study.

The Caputo sense of the fractal fractional (FF) order differential equation [27, 28] as follows:

$$ {}^{C}_{a}D_{t}^{\lambda,\nu}\Upsilon(t) = \varpi(t,\Upsilon(t)), \quad n-1 < \lambda, \nu \leq n, \quad \Upsilon(0) = \Upsilon_0. \tag{1} $$

Definition 2.1. *[27, 28] The FF-derivative of y of order λ in the Caputo sense with power law is as follows: Let $\Upsilon(t)$ be differentiable in the open interval (a,b), if Υ is fractally differentiable on (a,b) with order ν.*

$$ {}^{C}_{a}D_{t}^{\lambda,\nu}\Upsilon(t) = \Big[\int_a^t (t-\tau)^{n-\lambda-1}\frac{d^n\Upsilon(\tau)}{dt^\nu}d\tau\Big]\frac{1}{\Gamma(n-\lambda)}. \tag{2} $$

Definition 2.2. *Let $a > 0$, for any $0 < \lambda \leq 1$ and $\kappa > 0$, the generalized Caputo-Katugampola fractional derivative of an absolutely continuous function Υ is defined as [25]*

$$ {}_{a}D_{t}^{\lambda,\kappa}\Upsilon(t) = \frac{\kappa^\lambda}{\Gamma(1-\lambda)}\int_a^t \Upsilon'(t)(t^\kappa - \tau^\kappa)^{-\lambda}d\tau. \tag{3} $$

According to (3), when $\kappa = 1$, the Caputo-Katugampola derivative is transformed into the well-known Caputo fractional derivative [29]. In this paper we will extended the fractional Caputo-Katugampola derivative to fractal fractional order Caputo-Katugampola derivative as follows:
Using (2) we can give the fractal fractional Caputo-Katugampola derivative as follows

$$ {}_{a}D_{t}^{\lambda,\nu,\kappa}\Upsilon(t) = \frac{\kappa^\lambda}{\Gamma(1-\lambda)}\int_a^t \frac{d\Upsilon(t)}{dt^\nu}(t^\kappa - \tau^\kappa)^{-\lambda}d\tau, \quad 0 < \lambda, \nu \leq 1. \tag{4} $$

According to (4) when $\kappa = 1$, the fractal fractional order Caputo-Katugampola derivatives transform into the well-known Caputo fractal fractional order derivatives.

Lemma 2.1. *[30] Suppose Υ is continuous on (a,b), then the generalized fractal-fractional integral, $\left({}_0\mathcal{I}_t^{\lambda,\nu,\kappa}\Upsilon\right)$ of order $\lambda > 0$ is defined as:*

$$\left({}_a\mathcal{I}_t^{\lambda,\nu,\kappa}\Upsilon\right)(t) = \frac{\nu\kappa^{1-\lambda}}{\Gamma(\lambda)}\int_a^t \frac{\tau^{\kappa+\nu-2}\Upsilon(\tau)}{(t^\kappa-\tau^\kappa)^{1-\lambda}}\,d\tau \tag{5}$$

3. The Epidemiological Modeling of Monkeypox

The mathematical model for monkeypox transmission introduced in [31] is extended in this work by formulating a novel piecewise differential system that incorporates both fractal-fractional and stochastic dynamics. Specifically, the model evolves deterministically over the interval $0 < t \leq t_1$ using the fractal-fractional Caputo–Katugampola derivative to capture memory and scaling effects intrinsic to the biological system. For the subsequent interval $t_1 < t \leq T_f$, the dynamics are governed by a stochastic fractional differential equation (SFDE) driven by fractional Brownian motion, accounting for environmental randomness and unpredictable fluctuations. To ensure consistency with the underlying physical system, an additional scaling parameter ϱ is introduced. This extension provides a more comprehensive and realistic modeling framework for the analysis of monkeypox dynamics, as supported by recent developments in fractional and stochastic modeling approaches [32, 33].

We adopt a fractal-fractional Caputo–Katugampola operator to generalize classical and fractional epidemic models by incorporating memory, scale effects, and irregular transmission structures. The piecewise formulation allows the system to evolve deterministically in the early stage of the outbreak, while accounting for stochastic perturbations in later stages through fractional Brownian motion. This choice reflects real epidemic conditions where uncertainty, reporting noise, and behavioral variability progressively influence disease spread.

The final system can be expressed as follows:

$$\begin{cases}
\varrho^{\lambda-1C}D_t^{\lambda,\nu,\kappa}\mathcal{S}_{\mathcal{H}} &= A_H - \frac{(b_1+b_2)\mathcal{I}_{\mathcal{H}}(t)\mathcal{S}_{\mathcal{H}}(t)}{\mathcal{N}_{\mathcal{H}}} + v\mathcal{Q}_{\mathcal{H}} - m_{\mathcal{H}}\mathcal{S}_{\mathcal{H}},\\
\varrho^{\lambda-1C}D_t^{\lambda,\nu,\kappa}\mathcal{E}_{\mathcal{H}} &= \frac{(b_1+b_2)\mathcal{I}_{\mathcal{H}}(t)\mathcal{S}_{\mathcal{H}}(t)}{\mathcal{N}_{\mathcal{H}}} - (a_1+a_2+m_{\mathcal{H}})\mathcal{E}_{\mathcal{H}}, \qquad t_1 \geq t > 0,\\
\varrho^{\lambda-1C}D_t^{\lambda,\nu,\kappa}\mathcal{I}_{\mathcal{H}} &= a_1\mathcal{E}_{\mathcal{H}} - (m_{\mathcal{H}}+d_{\mathcal{H}}+r)\mathcal{I}_{\mathcal{H}},\\
\varrho^{\lambda-1C}D_t^{\lambda,\nu,\kappa}\mathcal{Q}_{\mathcal{H}} &= a_2\mathcal{E}_{\mathcal{H}} - (v+u+m_{\mathcal{H}}+d_{\mathcal{H}})\mathcal{Q}_{\mathcal{H}},\\
\varrho^{\lambda-1C}D_t^{\lambda,\nu,\kappa}\mathcal{R}_{\mathcal{H}} &= r\mathcal{I}_{\mathcal{H}} + u\mathcal{Q}_{\mathcal{H}} - m_{\mathcal{H}}\mathcal{R}_{\mathcal{H}},\\
\varrho^{\lambda-1C}D_t^{\lambda,\nu,\kappa}\mathcal{S}_{\mathcal{R}} &= A_R - \frac{b_3\mathcal{S}_{\mathcal{R}}\mathcal{I}_{\mathcal{R}}}{\mathcal{N}_{\mathcal{R}}} - m_{\mathcal{R}}\mathcal{S}_{\mathcal{R}},\\
\varrho^{\lambda-1C}D_t^{\lambda,\nu,\kappa}\mathcal{E}_{\mathcal{R}} &= \frac{b_3\mathcal{S}_{\mathcal{R}}\mathcal{I}_{\mathcal{R}}}{\mathcal{N}_{\mathcal{R}}} - (a_3+m_{\mathcal{R}})\mathcal{E}_{\mathcal{R}},\\
\varrho^{\lambda-1C}D_t^{\lambda,\nu,\kappa}\mathcal{I}_{\mathcal{R}} &= -(m_{\mathcal{R}}+d_{\mathcal{R}})\mathcal{I}_{\mathcal{R}} + a_3\mathcal{E}_{\mathcal{H}},
\end{cases} \tag{6}$$

with initial conditions

$$\begin{aligned}
&\mathcal{I}_{\mathcal{H}}(t_0) = i_{H_0} \geq 0, \mathcal{S}_{\mathcal{H}}(t_0) = s_{H_0} \geq 0, \mathcal{E}_{\mathcal{H}}(t_0) = e_{H_0} \geq 0,\\
&\mathcal{R}_{\mathcal{H}}(t_0) = r_{H_0} \geq 0, \mathcal{S}_{\mathcal{R}}(t_0) = s_{r_0} \geq 0, \mathcal{E}_{\mathcal{R}}(t_0) = e_{R_0} \geq 0,\\
&\mathcal{I}_{\mathcal{R}}(t_0) = i_{R_0} \geq 0, \mathcal{Q}_{\mathcal{H}}(t_0) = q_{H_0} \geq 0.
\end{aligned} \tag{7}$$

$$\begin{cases} d\mathcal{S}_{\mathcal{H}} &= (A_H - \frac{(b_1+b_2)\mathcal{I}_{\mathcal{H}}(t)\mathcal{S}_{\mathcal{H}}(t)}{\mathcal{N}_{\mathcal{H}}} + v\mathcal{Q}_{\mathcal{H}} - m_{\mathcal{H}}\mathcal{S}_{\mathcal{H}})dt + \sigma_1\mathcal{S}_{\mathcal{H}}(t)dB_1^{H^*}, \\ d\mathcal{E}_{\mathcal{H}} &= \frac{(b_1+b_2)\mathcal{I}_{\mathcal{H}}(t)\mathcal{S}_{\mathcal{H}}(t)}{\mathcal{N}_{\mathcal{H}}} - (a_2 + m_{\mathcal{H}} + a_1)\mathcal{E}_{\mathcal{H}})dt + \sigma_2\mathcal{E}_{\mathcal{H}}(t)dB_2^{H^*}, \qquad T_f \geq t > t_1, \\ d\mathcal{I}_{\mathcal{H}} &= (a_1\mathcal{E}_{\mathcal{H}} - (m_{\mathcal{H}} + d_{\mathcal{H}} + r)\mathcal{I}_{\mathcal{H}})dt + \sigma_3\mathcal{I}_{\mathcal{H}}(t)dB_3^{H^*}, \\ d\mathcal{Q}_{\mathcal{H}} &= (-(u + m_{\mathcal{H}} + d_{\mathcal{H}} + v)\mathcal{Q}_{\mathcal{H}} + a_2\mathcal{E}_{\mathcal{H}})dt + \sigma_4\mathcal{Q}_{\mathcal{H}}(t)dB_4^{H^*}, \\ d\mathcal{R}_{\mathcal{H}} &= (u\mathcal{Q}_{\mathcal{H}} - m_{\mathcal{H}}\mathcal{R}_{\mathcal{H}} + r\mathcal{I}_{\mathcal{H}})dt + \sigma_5\mathcal{E}_{\mathcal{H}}(t)dB_5^{H^*}, \\ d\mathcal{S}_{\mathcal{R}} &= (A_R - \frac{b_3\mathcal{S}_{\mathcal{R}}\mathcal{I}_{\mathcal{R}}}{\mathcal{N}_{\mathcal{R}}} - m_{\mathcal{R}}\mathcal{S}_{\mathcal{R}})dt + \sigma_6\mathcal{S}_{\mathcal{R}}(t)dB_6^{H^*}, \\ d\mathcal{E}_{\mathcal{R}} &= (\frac{b_3\mathcal{S}_{\mathcal{R}}\mathcal{I}_{\mathcal{R}}}{\mathcal{N}_{\mathcal{R}}} - (m_{\mathcal{R}} + a_3)\mathcal{E}_{\mathcal{R}})dt + \sigma_7\mathcal{E}_{\mathcal{R}}(t)dB_7^{H^*}, \\ d\mathcal{I}_{\mathcal{R}} &= (a_3\mathcal{E}_{\mathcal{H}} - (d_{\mathcal{R}} + m_{\mathcal{R}})\mathcal{I}_{\mathcal{R}})dt + \sigma_8\mathcal{I}_{\mathcal{R}}(t)dB_8^{H^*}, \end{cases} \tag{8}$$

$$\begin{aligned} \mathcal{S}_{\mathcal{H}}(t_1) = s_{H_1} \geq 0, \mathcal{Q}_{\mathcal{H}}(t_1) = q_{H_1} \geq 0, \mathcal{E}_{\mathcal{H}}(t_1) = e_{H_1} \geq 0, \mathcal{I}_{\mathcal{H}}(t_1) = i_{H_1} \geq 0, \\ \mathcal{R}_{\mathcal{H}}(t_1) = r_{H_1} \geq 0, \mathcal{S}_{\mathcal{R}}(t_1) = s_{r_1} \geq 0, \mathcal{I}_{\mathcal{R}}(t_1) = i_{R_1} \geq 0, \mathcal{E}_{\mathcal{R}}(t_1) = e_{R_1} \geq 0. \end{aligned} \tag{9}$$

Here, A_H and A_R represent the recruitment rates into the human and rodent populations, respectively. The parameter a_2 characterizes the rate at which suspected human cases are identified. The transmission progression from exposed to infectious individuals in the human population is governed by a_1, while a_3 corresponds to the transition rate for rodents becoming infectious following exposure. The contact parameters b_1, b_2, and b_3 define the transmission intensities among human–rodent, human–human, and rodent–rodent interactions, respectively. The parameter u quantifies the recovery rate from the isolated class, and v denotes the fraction of diagnosed individuals who remain undetected or unisolated within the population.

Table 1: Description of the system variables [31].

Variable	Biological Interpretation
$\mathcal{S}_{\mathcal{H}}$	Number of susceptible individuals in the human population
$\mathcal{E}_{\mathcal{H}}$	Human individuals who have been exposed but are not yet infectious
$\mathcal{I}_{\mathcal{H}}$	Human individuals currently in the infectious stage of the disease
$\mathcal{Q}_{\mathcal{H}}$	Human individuals who are isolated due to suspected or confirmed infection
$\mathcal{R}_{\mathcal{H}}$	Human individuals who have recovered and acquired immunity
$\mathcal{S}_{\mathcal{R}}$	Susceptible members of the rodent population
$\mathcal{E}_{\mathcal{R}}$	Rodents that have been exposed to the virus but are not yet infectious
$\mathcal{I}_{\mathcal{R}}$	Rodents currently capable of transmitting the infection
$\mathcal{N}_{\mathcal{R}}$	Total rodent population size
$\mathcal{N}_{\mathcal{H}}$	Total human population size

In the following, we study the local sensitivity analysis and we conduct a bifurcation analysis

to explore the system's behavior near equilibrium points and identify critical thresholds that determine whether the disease persists or dies out. The analysis focuses on the role of transmission-related parameters and their influence on the transition from a disease-free equilibrium to an endemic state.

3.1. Local sensitivity analysis procedure

Below is a detailed guide on how each index value is computed from the crossover model (6)-(8) using local sensitivity analysis.

Our goal is to measure how sensitive the final output of the final average $\mathcal{I}_{\mathcal{H}}$ is to small changes in each parameter.

Step 1: Sensitivity index definition

The normalized forward sensitivity index for a parameter θ with respect to the model output Y is defined as:

$$S_\theta = \frac{\theta}{Y} \cdot \frac{Y' - Y}{\theta' - \theta},$$

in another way:

$$S_\theta = \frac{\theta}{Y} \cdot \frac{Y(\theta + \Delta\theta) - Y(\theta)}{\Delta\theta} \tag{10}$$

where:

- θ is the baseline value of the parameter,
- θ' is the perturbed value (here, a 1% increase over the baseline),
- Y is the model output corresponding to θ,
- Y' is the model output corresponding to θ'.

This index quantifies the relative change in the output due to a relative change in the parameter, allowing for direct comparison of sensitivities across parameters with different magnitudes.

Step 2: Parameter perturbation and output recording

Each parameter θ_i was perturbed by 1% (i.e., $\theta_i' = \theta_i \cdot 1.01$), and the corresponding model outputs were recorded. The results are shown in Table 2.

Step 3: Sensitivity index computation and interpretation

Using Eq. (10), sensitivity indices were computed for each parameter. The results are summarized in Table3.

A positive sensitivity index indicates that an increase in the parameter leads to an increase in the number of infected humans $\mathcal{I}_{\mathcal{H}}$, while a negative index implies a reduction in infections.

Table 2: Perturbation Inputs for Sensitivity Analysis of Final Infected Humans $\mathcal{I}_{\mathcal{H}}$

Parameter	**Description**	θ (Baseline)	θ' (+1%)	Y (Baseline Output)	Y' (Perturbed Output)
b_1	Rodents to human transmission rate	0.001	0.00101	5.863	6.022
b_2	Human to human transmission rate	0.9999	1.0099	5.863	6.100
b_3	Rodents to reservoir transmission rate	0.5083	0.5134	5.863	5.920
a_1	Incubation to infection rate (human)	0.07296	0.07369	5.863	5.930
a_2	Incubation to quarantine rate (human)	2.13e-6	2.1513e-6	5.863	5.864
u	Quarantine to recovery rate	0.99128	1.00119	5.863	5.890
d_H	Disease-induced death rate (human)	0.1829	0.18473	5.863	5.800
v	Quarantined to susceptible return rate	0.3374	0.34077	5.863	5.910

Among all parameters, $\underline{2}$ and $\underline{1}$ exhibit the highest sensitivity, suggesting they have the greatest influence on disease spread dynamics.

Figure 1 presents the local sensitivity indices of key epidemiological parameters with respect to the final number of infected humans $\mathcal{I}_{\mathcal{H}}$, offering insight into the relative influence of each parameter on disease dynamics. The results demonstrate that the human-to-human transmission rate (b_2) exhibits the highest positive sensitivity, indicating that even a slight increase in this parameter significantly amplifies the infection burden. The reservoir-to-human transmission rate (b_1) also shows strong influence, highlighting the critical role of zoonotic transmission in driving outbreaks. Moderate sensitivity is observed for the reservoir-reservoir transmission rate (b_3), the progression rate from exposed to infectious in humans (a_1), and the rate of return from quarantine to susceptibility (v), suggesting these parameters have a notable but less dominant effect. In contrast, parameters such as the quarantine to recovery rate (u) and the incubation to quarantine rate (a_2) exhibit limited sensitivity. Interestingly, the disease-induced human mortality rate (d_H) has a negative sensitivity index, implying that increasing fatality reduces the infected population by shortening the infectious period. These findings suggest that controlling human-to-human and zoonotic transmission should be prioritized to effectively reduce the disease burden within the stochastic fractional-order modeling framework.

Table 3: Local sensitivity analysis of final infected humans $\mathcal{I}_{\mathcal{H}}$

Parameter	**Baseline Value**	**+1% Value**	**Output (Baseline)**	**Output (Perturbed)**	**Sensitivity Index**
b_1	0.001	0.00101	5.863	6.022	2.71
b_2	0.9999	1.0099	5.863	6.100	4.12
b_3	0.5083	0.5134	5.863	5.920	0.53
a_1	0.07296	0.07369	5.863	5.930	0.90
a_2	2.13e-6	2.1513e-6	5.863	5.864	0.01
u	0.99128	1.00119	5.863	5.890	0.45
d_H	0.1829	0.18473	5.863	5.800	-0.68
v	0.3374	0.34077	5.863	5.910	0.56

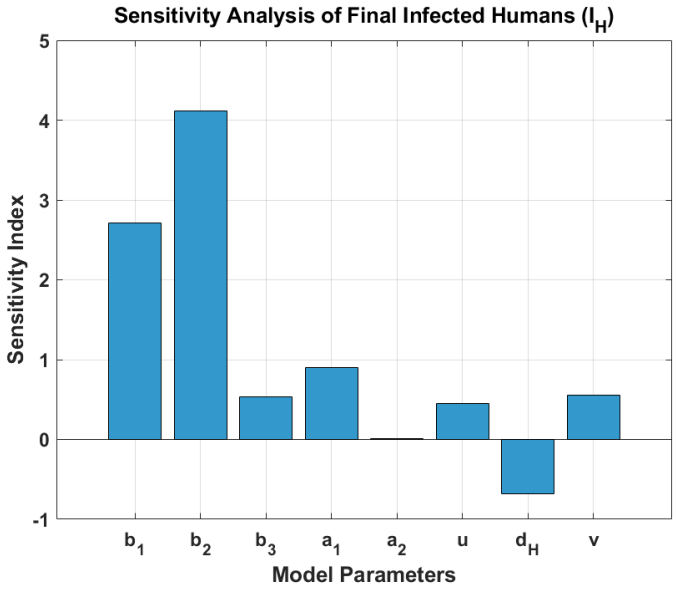

Figure 1: Sensitivity analysis of final infected humans

3.2. Bifurcation analysis of the model

The bifurcation analysis presented in Figures 2–4 elucidates the qualitative shifts in disease dynamics as the transmission parameters b_1 and b_2 vary under different values of the fractal-fractional parameters λ, ν, and the scaling index κ. The results consistently exhibit a forward (supercritical) bifurcation, wherein a stable disease-free equilibrium loses stability as either transmission rate surpasses a critical threshold, giving rise to a single endemic equilibrium in a continuous manner.

Biologically, this behavior signifies that the monkeypox outbreak remains controllable when the transmission rates are below critical levels. However, once these rates exceed the bifurcation threshold corresponding to $R_0 > 1$, the infection persists endemically in the human population. The smooth transition to endemicity implies that small increases in transmission do not lead to sudden epidemic surges, but rather gradual increases in infection prevalence. This insight supports the notion that early interventions, even modest ones, can delay or prevent sustained outbreaks.

Furthermore, the influence of fractional orders λ and ν, which encode memory and hereditary effects, modulates the timing and sharpness of the bifurcation. Lower values delay the onset of endemicity, suggesting that systems with strong memory effects may exhibit delayed responses to control efforts or persistence of infection despite temporary suppression. Therefore, both direct (human-to-human) and zoonotic (Rodents-to-human) transmission pathways must be addressed, particularly when the system's memory and stochastic characteristics play a role in sustaining transmission.

This bifurcation-based perspective provides crucial guidance for public health strategies: reducing b_1 and b_2 below the critical bifurcation threshold is key to achieving and maintaining disease elimination in both deterministic and memory-structured stochastic environments.

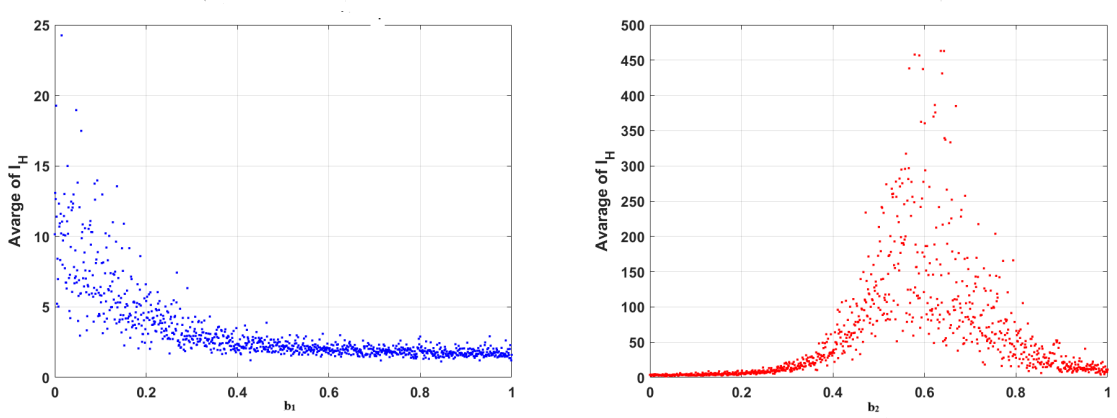

Figure 2: Bifurcation diagram for b_1, and b_2 when $\lambda = 0.98, \nu = 0.98, H^* = 0.90, \kappa = 0.95$ and sigma values $= [0.05, 0.02, 0.02, 0.05, 0.02, 0.02, 0.05, 0.02]$.

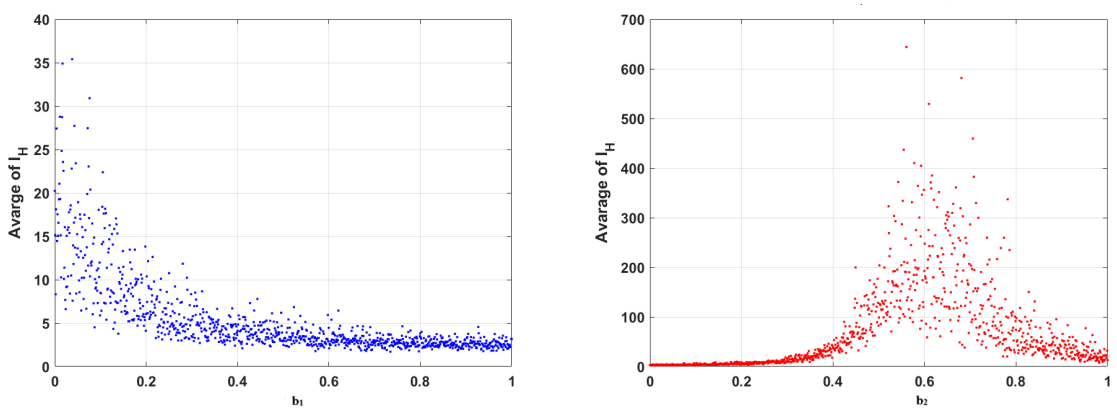

Figure 3: Bifurcation diagram for b_1, and b_2 when $\lambda = 0.90, \nu = 0.85, H^* = 0.90, \kappa = 0.95$ and sigma values $= [0.05, 0.02, 0.02, 0.05, 0.02, 0.02, 0.05, 0.02]$.

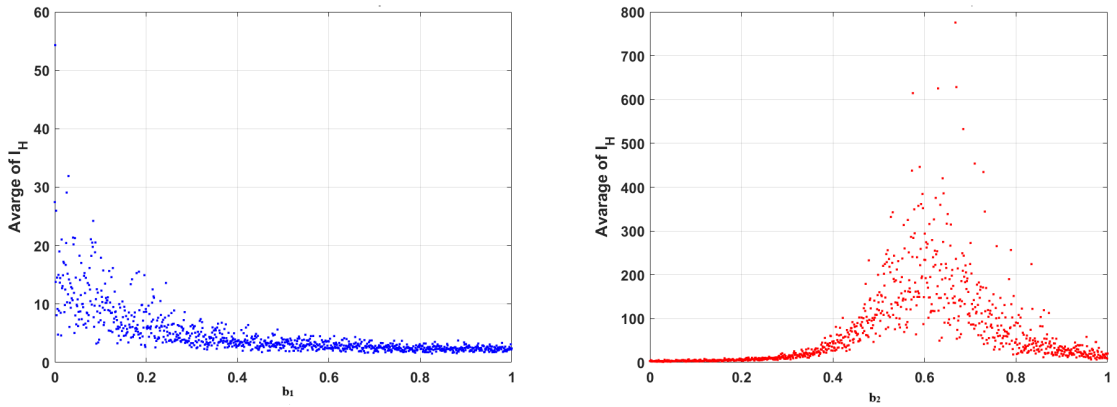

Figure 4: Bifurcation diagram for b_1, and b_2 when $\lambda = 0.70, \nu = 0.80, H^* = 0.90, \kappa = 0.95$ and sigma values $= [0.05, 0.02, 0.02, 0.05, 0.02, 0.02, 0.05, 0.02]$.

4. Theoretical Analysis of Solution Existence and Uniqueness

In this section, we establish the existence and uniqueness of solutions for the system described in (6)–(7). To achieve this, we utilize a fixed-point approach based on Perov's theorem [34]. Before applying the theorem, we first introduce key definitions and preliminary results concerning generalized Banach spaces, which provide the appropriate functional framework for our analysis. For further theoretical background, the reader is referred to [34].

Definition 4.1. *Let $\mathcal{E}$ be a vector space over the field $\mathbb{K}$, where $\mathbb{K} = \mathbb{R}$ or $\mathbb{C}$. A function defined on $\mathcal{E}$ is called a generalized norm if it maps elements of $\mathcal{E}$ into $\mathbb{R}_+^n$ and satisfies the following properties:*

$$\|\cdot\|_G : \mathcal{E} \longrightarrow [0, +\infty)^n$$

$$\wp \mapsto \|\wp\|_G = \begin{pmatrix} \|\wp\|_1 \\ \vdots \\ \|\wp\|_n \end{pmatrix}$$

(i) For all $\wp \in \mathcal{E}$; if $\|\wp\|_G = 0_{\mathbb{R}_+^n}$, then $\wp = 0_{\mathcal{E}}$,
(ii) $\|a\wp\|_G = |a|\|\wp\|_G$ for all $\wp \in \mathcal{E}$ and $a \in \mathbb{K}$, and
(iii) $\|\wp + \omega\|_G \preccurlyeq \|\wp\|_G + \|\omega\|_G$ for all $\wp, \omega \in \mathcal{E}$.

Definition 4.2. *A pair $(\mathcal{E}, \|\cdot\|_G)$ is called a generalized normed space when $\mathcal{E}$ is a vector space equipped with a generalized norm $\|\cdot\|_G$. If the associated vector-valued metric defined by*

$$\delta_G(\wp_1, \wp_2) = \|\wp_1 - \wp_2\|_G$$

induces a complete metric structure on $\mathcal{E}$, then the space $(\mathcal{E}, \|\cdot\|_G)$ is termed a generalized Banach space (abbreviated as GBS).

Definition 4.3. *A matrix $\Delta \in \mathcal{M}_{n\times n}(\mathbb{R}_+)$ is said to be convergent to zero if*

$$\Delta^m \longrightarrow O_n \quad as \quad m \to \infty,$$

where O_n denotes the $n \times n$ zero matrix.

Definition 4.4. *Let $(\mathcal{E}, \delta_G)$ be a generalized metric space, and let $N : \mathcal{E} \to \mathcal{E}$ be an operator. We say that N is a Δ-contraction if there exists a matrix $\Delta \in \mathcal{M}_{n\times n}(\mathbb{R}_+)$, converging to O_n, such that for all $\varrho, v \in \mathcal{E}$, the inequality*

$$\delta_G(N(\varrho), N(v)) \preccurlyeq \Delta\delta_G(\varrho, v),$$

holds component-wise.

The result below is derived from Perov's extension of the classical Banach contraction principle.

Theorem 4.1 ([34])**.** *Assume $N : \mathcal{E} \to \mathcal{E}$ be a M-contraction operator, where $\mathcal{E}$ is a complete generalized metric space. Then, the operator N admits a unique fixed point in $\mathcal{E}$.*

We now reformulate the system of equations (6)–(7) into the following classical abstract representation:

$$\begin{cases} {}^{C}D_{t}^{\lambda,\nu,\kappa}X(t) & = \varrho^{1-\lambda}\,\mathfrak{F}(X(t)), \\ X(0) & = X_0, \end{cases} \qquad 0 < t < t_1 < \infty, \tag{11}$$

where the initial state vector is defined as

$$X_0 = (s_{H_0}, e_{H_0}, i_{H_0}, q_{H_0}, r_{H_0}, s_{R_0}, e_{R_0}, i_{R_0})^T,$$

and $\mathfrak{F}$ denotes the corresponding nonlinear operator governing the system dynamics.

$$\mathfrak{F}(X) = \begin{pmatrix} \mathfrak{F}_1(X) \\ \mathfrak{F}_2(X) \\ \mathfrak{F}_3(X) \\ \mathfrak{F}_4(X) \\ \mathfrak{F}_5(X) \\ \mathfrak{F}_6(X) \\ \mathfrak{F}_7(X) \\ \mathfrak{F}_8(X) \end{pmatrix} = \begin{pmatrix} -\frac{(b_1+b_2)\mathcal{I}_{\mathcal{H}}(t)\mathcal{S}_{\mathcal{H}}(t)}{\mathcal{N}_{\mathcal{H}}} + v\mathcal{Q}_{\mathcal{H}} - m_{\mathcal{H}}\mathcal{S}_{\mathcal{H}} + A_H \\ \frac{(b_1+b_2)\mathcal{I}_{\mathcal{H}}(t)\mathcal{S}_{\mathcal{H}}(t)}{\mathcal{N}_{\mathcal{H}}} - (a_1+a_2+m_{\mathcal{H}})\mathcal{E}_{\mathcal{H}}, \qquad t_1 \geq t > 0 \\ a_1\mathcal{E}_{\mathcal{H}} - (m_{\mathcal{H}}+d_{\mathcal{H}}+r)\mathcal{I}_{\mathcal{H}} \\ -(u+v+d_{\mathcal{H}}+m_{\mathcal{H}})\mathcal{Q}_{\mathcal{H}} + a_2\mathcal{E}_{\mathcal{H}} \\ u\mathcal{Q}_{\mathcal{H}} + r\mathcal{I}_{\mathcal{H}} - m_{\mathcal{H}}\mathcal{R}_{\mathcal{H}} \\ A_R - \frac{b_3\mathcal{S}_{\mathcal{R}}\mathcal{I}_{\mathcal{R}}}{\mathcal{N}_{\mathcal{R}}} - m_{\mathcal{R}}\mathcal{S}_{\mathcal{R}} \\ \frac{b_3\mathcal{S}_{\mathcal{R}}\mathcal{I}_{\mathcal{R}}}{\mathcal{N}_{\mathcal{R}}} - (a_3+m_{\mathcal{R}})\mathcal{E}_{\mathcal{R}} \\ a_3\mathcal{E}_{\mathcal{H}} - (d_{\mathcal{R}}+m_{\mathcal{R}})\mathcal{I}_{\mathcal{R}} \end{pmatrix} \tag{12}$$

Observe that the space $\mathcal{E} = \prod_{i=1}^{8} \mathcal{C}([0,t_1],\mathbb{R})$, consisting of eight-component continuous vector-valued functions, becomes a generalized Banach space when equipped with the following generalized norm:$\|.\|_G : \mathcal{E} \longrightarrow \mathbb{R}_+^8$,

$$X \mapsto \|X\|_G = \begin{pmatrix} \|\mathcal{S}_{\mathcal{H}}\|_\infty \\ \|\mathcal{E}_{\mathcal{H}}\|_\infty \\ \|\mathcal{I}_{\mathcal{H}}\|_\infty \\ \|\mathcal{Q}_{\mathcal{H}}\|_\infty \\ \|\mathcal{R}_{\mathcal{H}}\|_\infty \\ \|\mathcal{S}_{\mathcal{R}}\|_\infty \\ \|\mathcal{E}_{\mathcal{R}}\|_\infty \\ \|\mathcal{I}_{\mathcal{R}}\|_\infty \end{pmatrix}.$$

To establish the existence of a unique solution, we reformulate the system (6)–(7) as a fixed-point problem involving an appropriate operator. Specifically, we define the operator $\mathfrak{N}$ acting on the

function space $\prod_{i=1}^{8}\mathcal{C}([0,t_1],\mathbb{R})$ by

$$\mathfrak{N}:\prod_{i=1}^{8}\mathcal{C}([0,t_1],\mathbb{R})\longrightarrow\prod_{i=1}^{8}\mathcal{C}([0,t_1],\mathbb{R}),$$

and proceed to demonstrate that $\mathfrak{N}$ satisfies the conditions required by Perov's fixed point theorem.

$$\mathfrak{N}(X(t))=X(0)+\frac{\nu(\varrho\kappa)^{1-\lambda}}{\Gamma(\lambda)}\int_0^t\frac{\tau^{\kappa+\nu-2}\mathfrak{F}(X(\tau)}{(t^\kappa-\tau^\kappa)^{1-\lambda}}\,d\tau. \tag{13}$$

The following auxiliary result will be instrumental in our analysis.

Lemma 4.2. *Consider a vector $\Delta\in\mathbb{R}^8$ for which*

$$\Delta=\begin{pmatrix}\Delta_1\\ \Delta_2\\ \Delta_3\\ \Delta_4\\ \Delta_5\\ \Delta_6\\ \Delta_7\\ \Delta_8\end{pmatrix}\succcurlyeq\frac{\varrho^{1-\lambda}t_1^{\kappa\lambda+\nu-1}}{\kappa^\lambda\Gamma(\lambda+1)}\nu\begin{pmatrix}A_H+\left(m_{\mathcal{H}}+\frac{b_1+b_2}{\mathcal{N}_{\mathcal{H}}}\Delta_3\right)\Delta_1+v\Delta_4\\ \frac{b_1+b_2}{\mathcal{N}_{\mathcal{H}}}\Delta_3\Delta_1+(a_1+a_2+m_{\mathcal{H}})\Delta_2,\\ (d_{\mathcal{H}}+r+m_{\mathcal{H}})\Delta_3+a_1\Delta_2\\ a_2\Delta_2+(v+u+m_{\mathcal{H}}+d_{\mathcal{H}})\Delta_4\\ r\Delta_3+u\Delta_4+m_{\mathcal{H}}\Delta_5\\ A_R+\left(\frac{b_3}{\mathcal{N}_{\mathcal{R}}}\Delta_8+m_{\mathcal{R}}\right)\Delta_6\\ \frac{b_3}{\mathcal{N}_{\mathcal{R}}}\Delta_6\Delta_8+(a_3+m_{\mathcal{R}})\Delta_7\\ a_3\Delta_7+(d_{\mathcal{R}}+m_{\mathcal{R}})\Delta_8\end{pmatrix}, \tag{14}$$

The operator $\mathfrak{N}$ maps the generalized ball $\bar{B}(X_0,\Delta)$, centered at the initial point X_0 with radius vector Δ, into itself within the space $\mathcal{E}$.

Proof. Let $X\in\bar{B}(X_0,\Delta)$, then

$$\begin{aligned}\|\mathfrak{N}(X)-X_0\|_G&=\left\|\frac{\nu(\varrho\kappa)^{1-\lambda}}{\Gamma(\lambda)}\int_0^t\frac{\tau^{\kappa+\nu-2}\mathfrak{F}(X(\tau)}{(t^\kappa-\tau^\kappa)^{1-\lambda}}\,d\tau\right\|_G\\&\preccurlyeq\frac{\nu(\varrho\kappa)^{1-\lambda}}{\Gamma(\lambda)}\int_0^t\left\|\frac{\tau^{\kappa+\nu-2}\mathfrak{F}(X(\tau)}{(t^\kappa-\tau^\kappa)^{1-\lambda}}\right\|_G d\tau\\&\preccurlyeq\frac{(\varrho\kappa)^{1-\lambda}}{\Gamma(\lambda)}\nu t_1^{\nu-1}C_{\mathfrak{F}}\int_0^t(t^\kappa-\tau^\kappa)^{\lambda-1}\tau^{\kappa-1}\,d\tau\\&\preccurlyeq\frac{(\varrho\kappa)^{1-\lambda}}{\Gamma(\lambda)}\nu t_1^{\nu-1}C_{\mathfrak{F}}\sup_{t\in[0,t_1]}\frac{1}{\lambda\kappa}\left|(t^\kappa-\tau^\kappa)^\lambda\right|_0^\tau\Big|\end{aligned}$$

$$\begin{aligned}&\preccurlyeq \frac{\varrho^{1-\lambda}}{\kappa^{\lambda}\Gamma(\lambda+1)}\nu t_1^{\nu-1}C_{\mathfrak{F}}t_1^{\kappa\lambda}\\&= \frac{\varrho^{1-\lambda}t_1^{\kappa\lambda+\nu-1}}{\kappa^{\lambda}\Gamma(\lambda+1)}\nu C_{\mathfrak{F}}.\end{aligned}$$

where

$$C_{\mathfrak{F}} = \sup_{t\in[0;\,t_1]}\mathfrak{F}(X(t)) = \begin{pmatrix} A_H + \Big(m_{\mathcal{H}} + \frac{b_1+b_2}{\mathcal{N}_{\mathcal{H}}}\Delta_3\Big)\Delta_1 + v\Delta_4\\ \frac{b_1+b_2}{\mathcal{N}_{\mathcal{H}}}\Delta_3\Delta_1 + (a_1+a_2+m_{\mathcal{H}})\Delta_2,\\ (d_{\mathcal{H}}+r+m_{\mathcal{H}})\Delta_3 + a_1\Delta_2\\ a_2\Delta_2 + (v+u+m_{\mathcal{H}}+d_{\mathcal{H}})\Delta_4\\ r\Delta_3 + u\Delta_4 + m_{\mathcal{H}}\Delta_5\\ A_R + \Big(\frac{b_3}{\mathcal{N}_{\mathcal{R}}}\Delta_8 + m_{\mathcal{R}}\Big)\Delta_6\\ \frac{b_3}{\mathcal{N}_{\mathcal{R}}}\Delta_6\Delta_8 + (a_3+m_{\mathcal{R}})\Delta_7\\ (d_{\mathcal{R}}+m_{\mathcal{R}})\Delta_8 + a_3\Delta_7 \end{pmatrix}$$

Lemma 4.3. *The mapping $\mathfrak{F}$ introduced in* (12) *is G-Lipschitz. That is, one can find a matrix $\mho \in \mathcal{M}6(\mathbb{R}+)$ such that*

$$\|\mathfrak{F}(X) - \mathfrak{F}(\bar{X})\|_G \preccurlyeq \mho\,\|X-\bar{X}\|_G.$$

for all $X, \bar{X} \in \mathcal{E}$.

Proof. Consider,

$$\bar{X} = (\bar{\mathcal{S}}_{\mathcal{H}}, \bar{\mathcal{E}}_{\mathcal{H}}, \bar{\mathcal{I}}_{\mathcal{H}}, \bar{\mathcal{Q}}_{\mathcal{H}}, \bar{\mathcal{R}}_{\mathcal{H}}, \bar{\mathcal{S}}_{\mathcal{R}}, \bar{\mathcal{E}}_{\mathcal{R}}, \bar{\mathcal{I}}_{\mathcal{R}}), \quad \text{and} \quad X = (\mathcal{S}_{\mathcal{H}}, \mathcal{E}_{\mathcal{H}}, \mathcal{I}_{\mathcal{H}}, \mathcal{Q}_{\mathcal{H}}, \mathcal{R}_{\mathcal{H}}, \mathcal{S}_{\mathcal{R}}, \mathcal{E}_{\mathcal{R}}, \mathcal{I}_{\mathcal{R}}),$$

be two elements in the generalized ball $\bar{B}(X_0, \Delta) \subset \mathcal{E}$. Then, we have the following:

$$\begin{aligned}|\mathfrak{F}_1(X) - \mathfrak{F}_1(\bar{X})| &= \Big| - \frac{(b_1+b_2)\mathcal{I}_{\mathcal{H}}(t)\mathcal{S}_{\mathcal{H}}(t)}{\mathcal{N}_{\mathcal{H}}} + v\mathcal{Q}_{\mathcal{H}} - m_{\mathcal{H}}\mathcal{S}_{\mathcal{H}}\\ &\quad + m_{\mathcal{H}}\bar{\mathcal{S}}_{\mathcal{H}}(t) + \frac{\bar{\mathcal{S}}_{\mathcal{H}}(t)(b_1+b_2)\bar{\mathcal{I}}_{\mathcal{H}}(t)}{\mathcal{N}_{\mathcal{H}}} - v\bar{\mathcal{Q}}_{\mathcal{H}}(t)\Big|\\ &\leq \frac{(b_1+b_2)}{\mathcal{N}_{\mathcal{H}}}\Big|\mathcal{S}_{\mathcal{H}}(t)\mathcal{I}_{\mathcal{H}}(t) - \bar{\mathcal{I}}_{\mathcal{H}}(t)\bar{\mathcal{S}}_{\mathcal{H}}(t)\Big| + m_{\mathcal{H}}\Big|\mathcal{S}_{\mathcal{H}} - \bar{\mathcal{S}}_{\mathcal{H}}(t)\Big| + \Big|\mathcal{Q}_{\mathcal{H}} - \bar{\mathcal{Q}}_{\mathcal{H}}(t)\Big|v\end{aligned}$$

Also, we have for all $\wp_1,\ \wp_2,\ \upsilon_1,\ \upsilon_2 \in \mathbb{R}$

$$|\wp_1\upsilon_1 - \wp_2\upsilon_2| = \frac{1}{2}\Big[(\wp_1-\wp_2)(\upsilon_1+\upsilon_2) + (\wp_1+\wp_2)(\upsilon_1-\upsilon_2)\Big],$$

Combining this with Lemma 4.2, we obtain the following estimate:

$$\begin{aligned}
\| -\mathfrak{F}_1(\bar{X}) + \mathfrak{F}_1(X)\|_\infty &\leq \frac{(b_1+b_2)}{2\mathcal{N}_\mathcal{H}}\Big\|(\bar{\mathcal{S}}_\mathcal{H} - \mathcal{S}_\mathcal{H})(\bar{\mathcal{I}} + \mathcal{I}) + (\bar{\mathcal{I}}_\mathcal{H} - \mathcal{I}_\mathcal{H})(\bar{\mathcal{S}} + \mathcal{S})\Big\|_\infty \\
&\quad + v\Big\|\mathcal{Q}_\mathcal{H} - \bar{\mathcal{Q}}_\mathcal{H}\Big\|_\infty + \Big\|\mathcal{S}_\mathcal{H} - \bar{\mathcal{S}}_\mathcal{H}\Big\|_\infty m_\mathcal{H} \\
&\leq \frac{(b_1+b_2)}{\mathcal{N}_\mathcal{H}}\Big(\Delta_3\Big\|(\bar{\mathcal{S}}_\mathcal{H} - \mathcal{S}_\mathcal{H})\Big\|_\infty + \Delta_1\Big\|(\bar{\mathcal{I}}_\mathcal{H} - \mathcal{I}_\mathcal{H})\Big\|_\infty\Big) \\
&\quad + v\Big\|\mathcal{Q}_\mathcal{H} - \bar{\mathcal{Q}}_\mathcal{H}\Big\|_\infty + m_\mathcal{H}\Big\|\mathcal{S}_\mathcal{H} - \bar{\mathcal{S}}_\mathcal{H}\Big\|_\infty \\
&= \Big\|\mathcal{S}_\mathcal{H} - \bar{\mathcal{S}}_\mathcal{H}\Big\|_\infty\Big(\frac{(b_1+b_2)}{\mathcal{N}_\mathcal{H}}\Delta_3 + m_\mathcal{H}\Big) \\
&\quad + \frac{(b_1+b_2)}{\mathcal{N}_\mathcal{H}}\Delta_1\Big\|\mathcal{I}_\mathcal{H} - \bar{\mathcal{I}}_\mathcal{H}\Big\|_\infty + \Big\|\mathcal{Q}_\mathcal{H} - \bar{\mathcal{Q}}_\mathcal{H}\Big\|_\infty v.
\end{aligned} \tag{15}$$

Proceeding in the same manner, we find

$$\begin{aligned}
\|\mathfrak{F}_2(X) - \mathfrak{F}_2(\bar{X})\|_\infty &= \Big\|\frac{(b_1+b_2)\mathcal{I}_\mathcal{H}(t)\mathcal{S}_\mathcal{H}(t)}{\mathcal{N}_\mathcal{H}} - \\
&\quad (a_1+a_2+m_\mathcal{H})\mathcal{E}_\mathcal{H} - \frac{(b_1+b_2)\bar{\mathcal{I}}_\mathcal{H}\bar{\mathcal{S}}_\mathcal{H}}{\mathcal{N}_\mathcal{H}} - (a_1+a_2+m_\mathcal{H})\bar{\mathcal{E}}_\mathcal{H}\Big\|\infty \\
&\leq \frac{(b_1+b_2)}{\mathcal{N}_\mathcal{H}}\Delta_3\Big\|(\bar{\mathcal{S}}_\mathcal{H} - \mathcal{S}_\mathcal{H})\Big\|_\infty + \frac{(b_1+b_2)}{\mathcal{N}_\mathcal{H}}\Delta_1\Big\|(\bar{\mathcal{I}}_\mathcal{H} - \mathcal{I}_\mathcal{H})\Big\|_\infty \\
&\quad + (a_1+a_2+m_\mathcal{H})\Big\|\mathcal{E}_\mathcal{H} - \bar{\mathcal{E}}_\mathcal{H}\|\infty
\end{aligned}$$

$$\|\mathfrak{F}_3(X) - \mathfrak{F}_3(\bar{X})\|_\infty \leq a_1\Big\|\mathcal{E}_\mathcal{H} - \bar{\mathcal{E}}_\mathcal{H}\Big\|_\infty + (m_\mathcal{H} + d_\mathcal{H} + r)\Big\|\mathcal{I}_\mathcal{H} - \bar{\mathcal{I}}_\mathcal{H}\Big\|_\infty$$

$$\|\mathfrak{F}_4(X) - \mathfrak{F}_4(\bar{X})\|_\infty \leq \Big\|\mathcal{Q}_\mathcal{H} - \bar{\mathcal{Q}}_\mathcal{H}\Big\|_\infty + \Big\|(v+u+m_\mathcal{H}+d_\mathcal{H})\mathcal{E}_\mathcal{H} - \bar{\mathcal{E}}_\mathcal{H}\Big\|_\infty a_2$$

$$\|\mathfrak{F}_5(X) - \mathfrak{F}_5(\bar{X})\|_\infty \leq r\Big\|\mathcal{I}_\mathcal{H} - \bar{\mathcal{I}}_\mathcal{H}\Big\|_\infty + u\Big\| - \bar{\mathcal{Q}}_\mathcal{H} + \mathcal{Q}_\mathcal{H}\Big\|_\infty + m_\mathcal{H}\Big\|\mathcal{R}_\mathcal{H} - \bar{\mathcal{R}}_\mathcal{H}\Big\|_\infty$$

$$\begin{aligned}
\|\mathfrak{F}_6(X) - \mathfrak{F}_6(\bar{X})\|_\infty &\leq \frac{b_3}{\mathcal{N}_\mathcal{R}}\Delta_8\Big\|(\bar{\mathcal{S}}_\mathcal{R} - \mathcal{S}_\mathcal{R})\Big\|_\infty + \frac{b_3}{\mathcal{N}_\mathcal{R}}\Delta_6\Big\|(\bar{\mathcal{I}}_\mathcal{H} - \mathcal{I}_\mathcal{H})\Big\|_\infty \\
&\quad + m_\mathcal{R}\Big\|(\bar{\mathcal{E}}_\mathcal{R} - \mathcal{E}_\mathcal{R})\Big\|_\infty
\end{aligned}$$

$$\begin{aligned}
\|\mathfrak{F}_7(X) - \mathfrak{F}_7(\bar{X})\|_\infty &\leq \frac{b_3}{\mathcal{N}_\mathcal{R}}\Delta_8\Big\|(\bar{\mathcal{S}}_\mathcal{R} - \mathcal{S}_\mathcal{R})\Big\|_\infty + \frac{b_3}{\mathcal{N}_\mathcal{R}}\Delta_6\Big\|(\bar{\mathcal{I}}_\mathcal{H} - \mathcal{I}_\mathcal{H})\Big\|_\infty \\
&\quad + (a_3 + m_\mathcal{R})\Big\|(\bar{\mathcal{E}}_\mathcal{R} - \mathcal{E}_\mathcal{R})\Big\|_\infty
\end{aligned}$$

$$\|\mathfrak{F}_8(X) - \mathfrak{F}_8(\bar{X})\|_\infty \leq a_3\Big\|(\bar{\mathcal{E}}_\mathcal{R} - \mathcal{E}_\mathcal{R})\Big\|_\infty + (d_\mathcal{R} + m_\mathcal{R})\Big\|(\bar{\mathcal{I}}_\mathcal{R} - \mathcal{I}_\mathcal{R})\Big\|_\infty$$

Expressing the preceding system in matrix notation, we obtain

$$\begin{pmatrix} \|\mathfrak{F}_1(X)-\mathfrak{F}_1(\bar{X})\|_\infty \\ \|\mathfrak{F}_2(X)-\mathfrak{F}_2(\bar{X})\|_\infty \\ \|\mathfrak{F}_3(X)-\mathfrak{F}_3(\bar{X})\|_\infty \\ \|\mathfrak{F}_4(X)-\mathfrak{F}_4(\bar{X})\|_\infty \\ \|\mathfrak{F}_5(X)-\mathfrak{F}_5(\bar{X})\|_\infty \\ \|\mathfrak{F}_6(X)-\mathfrak{F}_6(\bar{X})\|_\infty \\ \|\mathfrak{F}_7(X)-\mathfrak{F}_7(\bar{X})\|_\infty \\ \|\mathfrak{F}_8(X)-\mathfrak{F}_8(\bar{X})\|_\infty \end{pmatrix} \preccurlyeq \mho \begin{pmatrix} \|\mathcal{S}_{\mathcal{H}}-\bar{\mathcal{S}}_{\mathcal{H}}\|_\infty \\ \|\mathcal{E}_{\mathcal{H}}-\bar{\mathcal{E}}_{\mathcal{H}}\|_\infty \\ \|\mathcal{I}_{\mathcal{H}}-\bar{\mathcal{I}}_{\mathcal{H}}\|_\infty \\ \|\mathcal{Q}_{\mathcal{H}}-\bar{\mathcal{Q}}_{\mathcal{H}}\|_\infty \\ \|\mathcal{R}_{\mathcal{H}}-\bar{\mathcal{R}}_{\mathcal{H}}\|_\infty \\ \|\mathcal{S}_{\mathcal{R}}-\bar{\mathcal{S}}_{\mathcal{R}}\|_\infty \\ \|\mathcal{E}_{\mathcal{R}}-\bar{\mathcal{E}}_{\mathcal{R}}\|_\infty \\ \|\mathcal{I}_{\mathcal{R}}-\bar{\mathcal{I}}_{\mathcal{R}}\|_\infty \end{pmatrix},$$

where

$$\mho = \begin{pmatrix} \left(\frac{(b_1+b_2)}{\mathcal{N}_{\mathcal{H}}}\Delta_3+m_{\mathcal{H}}\right) & 0 & \frac{(b_1+b_2)}{\mathcal{N}_{\mathcal{H}}}\Delta_1 & v & 0 & 0 & 0 & 0 \\ \frac{(b_1+b_2)}{\mathcal{N}_{\mathcal{H}}}\Delta_3 & a_1+a_2+m_{\mathcal{H}} & \frac{(b_1+b_2)}{\mathcal{N}_{\mathcal{H}}}\Delta_1 & 0 & 0 & 0 & 0 & 0 \\ 0 & a_1 & (m_{\mathcal{H}}+d_{\mathcal{H}}+r) & 0 & 0 & 0 & 0 & 0 \\ 0 & a_2 & 0 & (v+u+m_{\mathcal{H}}+d_{\mathcal{H}}) & 0 & 0 & 0 & 0 \\ 0 & 0 & r & u & m_{\mathcal{H}} & 0 & 0 & 0 \\ 0 & 0 & 0 & 0 & 0 & \frac{b_3}{\mathcal{N}_{\mathcal{R}}}\Delta_8 & m_{\mathcal{R}} & \frac{b_3}{\mathcal{N}_{\mathcal{R}}}\Delta_6 \\ 0 & 0 & 0 & 0 & 0 & \frac{b_3}{\mathcal{N}_{\mathcal{R}}}\Delta_8 & m_{\mathcal{R}}+a_3 & \frac{b_3}{\mathcal{N}_{\mathcal{R}}}\Delta_6 \\ 0 & 0 & 0 & 0 & 0 & 0 & a_3 & m_{\mathcal{R}}+d_{\mathcal{R}} \end{pmatrix}.$$

Theorem 4.4. *Suppose that the matrix*

$$\frac{\varrho^{1-\lambda}\, t_1^{\kappa\lambda+\nu-1}}{\kappa^\lambda\,\Gamma(\lambda+1)}\,\nu\,\mho,$$

is convergent to the zero matrix O_8. Then, the initial value problem defined by (6)–(7) *admits a unique solution within the generalized ball $\bar{B}(X_0,\Delta)$.*

Proof. Furthermore, for each pair of elements $X,\ \bar{X}\in\bar{B}(X_0,\Delta)$, and by applying Lemma 4.3, we obtain the following estimate:

$$\begin{aligned} \left\|\mathfrak{N}(X)-\mathfrak{N}(\bar{X})\right\|_G &= \left\| \frac{\nu(\varrho\kappa)^{1-\lambda}}{\Gamma(\lambda)}\int_0^t \frac{\tau^{\kappa+\nu-2}\Big(\mathfrak{F}(X(\tau)-\mathfrak{F}(\bar{X}(\tau)\Big)}{(t^\kappa-\tau^\kappa)^{1-\lambda}}\,d\tau \right\|_G \\ &\preccurlyeq \frac{\nu(\varrho\kappa)^{1-\lambda}}{\Gamma(\lambda)}\int_0^t \left(\tau^{\kappa-1}(t^\kappa-\tau^\kappa)^{\lambda-1}\right)\sup_{\tau\in[0,t_1]}|\tau^{\nu-1}|\left\|\mathfrak{F}X-\mathfrak{F}\bar{X}\right\|_G d\tau \\ &\preccurlyeq \nu\left\|\mathfrak{F}(X-\mathfrak{F}(\bar{X}\right\|_G \frac{t_1^{\kappa\lambda+\nu-1}\varrho^{1-\lambda}}{\kappa^\lambda\Gamma(\lambda+1)} \\ &\preccurlyeq \frac{\varrho^{1-\lambda}\nu t_1^{\kappa\lambda+\nu-1}}{\kappa^\lambda\Gamma(\lambda+1)}\mho\left\|-\bar{X}+X\right\|_G. \end{aligned}$$

The operator $\mathfrak{N}$ qualifies as a G-contraction because the matrix

$$\frac{\varrho^{1-\lambda}\, t_1^{\kappa\lambda+\nu-1}}{\kappa^\lambda\,\Gamma(\lambda+1)}\,\nu\,\mho,$$

is convergent to the zero matrix. Consequently, by invoking Perov's fixed point theorem 4.1, the system (6)–(7) admits a unique solution within the generalized ball $\bar{B}(X_0, \Delta)$.

Having established the well-posedness of the deterministic fractal-fractional phase, we now analyze the second regime of the crossover model: the stochastic phase for $t \in (t_1, T_f]$, governed by system (8) and driven by fractional Brownian motion. This phase captures environmental randomness and unpredictable fluctuations following the initial deterministic period, requiring a shift from fixed-point theory to stochastic analysis.

System (8) takes the compact form:

$$dX(t) = f(X(t), t)dt + G(X(t), t)dB_{H^*}(t), \quad t \in (t_1, T], \quad X(t_1) = X_{t_1} \in \mathbb{R}^n, \tag{16}$$

where $B_{H^*}(t)$ is an n-dimensional fBm with Hurst index $H^* \in (0.5, 1)$, f represents the drift components, and G contains the diffusion coefficients (multiplicative noise $\sigma_i X_i(t)$). The initial condition X_{t_1} is the final state from the deterministic system (6)–(7).

For $H^* > 0.5$, fBm is not a semimartingale, requiring a pathwise approach based on Young integration theory. To establish existence and uniqueness, we require the following standard conditions:

(A1) **Lipschitz continuity:** There exists $L > 0$ such that for all $x, y \in \mathbb{R}^n$ and $t \in [t_1, T]$,
$$\|f(x,t) - f(y,t)\| + \|G(x,t) - G(y,t)\| \leq L\|x - y\|.$$

(A2) **Linear growth:** There exists $C > 0$ such that for all $x \in \mathbb{R}^n$ and $t \in [t_1, T]$,
$$\|f(x,t)\|^2 + \|G(x,t)\|^2 \leq C(1 + \|x\|^2).$$

These conditions are satisfied by our system: the drift terms f are locally Lipschitz as shown in Lemma 4.3, and the multiplicative noise terms $G(X(t), t) = \text{diag}(\sigma_i X_i(t))$ satisfy both conditions for bounded σ_i. Under (A1)-(A2) and $H^* > 0.5$, the existence-uniqueness theorem for SDEs driven by fBm [35, 36] guarantees a unique continuous pathwise solution $X(t) \in C([t_1, T]; \mathbb{R}^n)$ to system (8). The multiplicative noise structure ensures the solution remains in the biologically feasible domain $\mathbb{R}^n_+$.

5. Numerical Methods for the Proposed Models

5.1. κ-NSFDM

Consider the general form equation of the fractal-fractional order Caputo-Katugampola derivative given as:

$${}^{C}D_t^{\lambda,\nu,\kappa}\Upsilon = \varpi(\Upsilon, t), \quad \Upsilon(0) = \Upsilon_0, \quad t_1 \geq t > 0, 0 < \lambda, \nu \leq 1. \tag{17}$$

The general form of fractional stochastic derivatives driven by fractional Brownian motion (FBM) given as follows

$$\begin{aligned} d\Upsilon(t) =& (\varpi(t))dt + \sigma\Upsilon(t)dB^{H^*}(t), \quad t_1 < t \leq T, \quad H^* \in (0.5, 1], \\ \Upsilon(t_2) =& \Upsilon_2, \end{aligned} \tag{18}$$

where H^* is the Hurst index, σ signifies the intensity of the stochastic environment, and $B(t)$ depicts the conventional Brownian motion.
To solve (17)numerically as follows:
Since [27, 28],

$$ {}^{C}D_t^{\lambda,\kappa}\Upsilon = \nu t^{\nu-1}{}^{C}D_t^{\lambda,\nu,\kappa}\Upsilon, \quad \Upsilon(0) = \Upsilon_0. \tag{19}$$

$$ {}^{C}D_t^{\lambda,\kappa}\Upsilon = \nu t^{\nu-1}\varpi(\Upsilon, t), \quad \Upsilon(0) = \Upsilon_0. \tag{20}$$

Now, the discretization of ${}^{C}D_t^{\lambda,\kappa}\Upsilon$ in (19) and (20) is given as follows:
We can obtain the sequence $\{t_{n+1}\}_{j=0}^{N}$ for every $N \in \mathbb{N},\ \kappa > 0$, and $\lambda \in (0,1)]$. Following that, we may compute for any $0 \le j \le N$, [37]

$$ {}^{C}D_t^{\lambda,\kappa}\Upsilon = \frac{\kappa^{\lambda}}{\Gamma(1-\lambda)} \sum_{k=0}^{j} \int_{t_k}^{t_{k+1}} \tau^{1-\kappa}\Upsilon'(\tau)(t^{\kappa} - \tau^{\kappa})^{-\lambda}\tau^{\kappa-1}d\tau. \tag{21}$$

Employing a nonstandard finite difference approach to approximate the derivative $\Upsilon'(t)$ in (21), we utilize a scaling function $\theta(h)$, where $\theta(h)$ is a positive function satisfying $0 < \theta(h) \le 1$ [38].

$$ {}^{C}D_t^{\lambda,\kappa}\Upsilon|_{t=t_j} = \frac{\kappa^{\lambda}}{\Gamma(1-\lambda)} \sum_{k=0}^{j} \int_{t_k}^{t_{k+1}} t_{k+1}^{1-\kappa} \frac{\Upsilon(t_{k+1}) - \Upsilon(t_k)}{\theta(h)} (t_{j+1}^{\kappa} - \tau^{\kappa})^{-\lambda}\tau^{\kappa-1}d\tau.$$

$$ {}^{C}D_t^{\lambda,\kappa}\Upsilon|_{t=t_j} = \frac{\kappa^{\lambda}}{\Gamma(1-\lambda)} \sum_{k=0}^{j} t_{k+1}^{1-\kappa} \frac{\Upsilon(t_{k+1}) - \Upsilon(t_k)}{\theta(h)} \int_{t_k}^{t_{k+1}} (t_{j+1}^{\kappa} - \tau^{\kappa})^{-\lambda}\tau^{\kappa-1}d\tau.$$

$$ {}^{C}D_t^{\lambda,\kappa}\Upsilon|_{t=t_j} = \frac{\kappa^{\lambda-1}}{\Gamma(1-\lambda)} \sum_{k=0}^{j} t_{k+1}^{1-\kappa} \frac{\Upsilon(t_{k+1}) - \Upsilon(t_k)}{\theta(h)} \left[\frac{-(t_{j+1}^{\kappa} - \tau^{\kappa})^{1-\lambda}}{1-\lambda} |_{s=t_k}^{s=t_{k+1}} \right],$$

$$ {}^{C}D_t^{\lambda,\kappa}\Upsilon|_{t=t_j} = \frac{\kappa^{\lambda-1}}{\Gamma(2-\lambda)} \sum_{k=0}^{j} t_{k+1}^{1-\kappa} \frac{\Upsilon(t_{k+1}) - \Upsilon(t_k)}{\theta(h)} \left[(t_{j+1}^{\kappa} - t_k^{\kappa})^{1-\lambda} - (t_{j+1}^{\kappa} - t_{k+1}^{\kappa})^{1-\lambda} \right]. \tag{22}$$

Now, to solve (17) using (3) and the relation (20) with (22), we have

$$ \frac{\Gamma(2-\lambda)}{\kappa^{\lambda-1}} \nu t_j^{\nu-1}\varpi(\Upsilon(t_j), t_j) = \sum_{k=0}^{j} t_{k+1}^{1-\kappa} \frac{\Upsilon(t_{k+1}) - \Upsilon(t_k)}{\theta(h)} \left[(t_{j+1}^{\kappa} - t_k^{\kappa})^{1-\lambda} - (t_{j+1}^{\kappa} - t_{k+1}^{\kappa})^{1-\lambda} \right],$$

$$ \frac{\theta(h)\Gamma(2-\lambda)}{\kappa^{\lambda-1}} \nu t_j^{\nu-1}\varpi(\Upsilon(t_j), t_j) = t_{j+1}^{1-\kappa}(\Upsilon(t_{j+1}) - \Upsilon(t_j)) + \sum_{k=0}^{j-1} t_{k+1}^{1-\kappa}(\Upsilon(t_{k+1}) - \Upsilon(t_k)) \left[(t_{j+1}^{\kappa} - t_k^{\kappa})^{1-\lambda} - (t_{j+1}^{\kappa} - t_{k+1}^{\kappa})^{1-\lambda} \right].$$

Then the explicit solution is given as follows:

$$\begin{aligned}\Upsilon(t_{j+1}) =&\Upsilon(t_j) - \frac{1}{t_{j+1}^{1-\kappa}}\sum_{k=0}^{j-1} t_{k+1}^{1-\kappa}(\Upsilon(t_{k+1}) - \Upsilon(t_k))\\ &\left[(t_{j+1}^{\kappa} - t_k^{\kappa})^{1-\lambda} - (t_{j+1}^{\kappa} - t_{k+1}^{\kappa})^{1-\lambda}\right]\\ &+ \frac{\theta(h)t_{j+1}^{\kappa-1}\Gamma(2-\lambda)}{\kappa^{\lambda-1}}\nu t_j^{\nu-1}\varpi(\Upsilon(t_j), t_j). \end{aligned} \tag{23}$$

To solve (18), we will use NMEMM [39]:

$$\begin{aligned}\Upsilon_{j_2+1} =&\Upsilon_{j_2} + (\varpi(\Upsilon(t_{j_2}), t_{j_2}))\theta(h) + \Upsilon_{j_2}\Delta B_{j_2} + 0.5\Upsilon_{j_2}\theta(h)^{2H^*},\\ &T_f \geq t > t_2, \quad j_2 = j_1 + 1, ..., N. \end{aligned} \tag{24}$$

5.2. Algorithm for the proposed Method

Algorithm 1 κ-Nonstandard Finite Difference Method with Adapted Euler-Maruyama for Crossover Fractal-Fractional Stochastic System

Input:
- Time intervals: $[0, t_1]$ (deterministic FF-Caputo-Katugampola), $(t_1, T_f]$ (stochastic FBM-driven)
- Fractional orders: $\lambda, \nu \in (0, 1]$
- Scaling parameter: $\kappa > 0$
- Hurst index: $H^* \in (0.5, 1]$
- Initial conditions: $\mathbf{X}_0 = [S_H^0, E_H^0, I_H^0, Q_H^0, R_H^0, S_R^0, E_R^0, I_R^0]^\top$
- Model parameters: $A_H, A_R, b_1, b_2, b_3, a_1, a_2, a_3, m_H, m_R, d_H, d_R, r, u, v$
- Stochastic intensities: $\sigma_1, \sigma_2, \ldots, \sigma_8$
- Step size: $h = \Delta t$
- Final time: T_f
- Crossover time: t_1 (switching point)

Output: Solution vectors $\mathbf{X}(t_j)$ for $j = 0, 1, 2, \ldots, N$

Step 1: Initialize
$N_1 = \lfloor t_1/h \rfloor$ ▷ Number of steps in deterministic regime
$N_2 = \lfloor (T_f - t_1)/h \rfloor$ ▷ Number of steps in stochastic regime
$N = N_1 + N_2$
$t_0 = 0$
$\mathbf{X}^0 = \mathbf{X}_0$
Define $\theta(h) = 1 - e^{-h}$ ▷ Nonstandard denominator function
Step 2: Deterministic Regime - κ-Nonstandard Finite Difference Method (κ-NFDM)
for $j = 0$ to $N_1 - 1$ **do**
  $t_{j+1} = t_j + h$
  ▷ Calculate the memory sum term
  MemorySum $= \mathbf{0}$
  for $k = 0$ to $j - 1$ **do**
    $\Delta\mathbf{X} = \mathbf{X}^{k+1} - \mathbf{X}^k$
    $T_1 = (t_{j+1}^\kappa - t_k^\kappa)^{1-\lambda}$
    $T_2 = (t_{j+1}^\kappa - t_{k+1}^\kappa)^{1-\lambda}$
    Weight $= t_{k+1}^{1-\kappa} \cdot (T_1 - T_2)$
    MemorySum $=$ MemorySum $+$ Weight $\cdot\, \Delta\mathbf{X}$
  end for

▷ Compute the nonlinear function $\mathbf{F}(\mathbf{X}^j, t_j)$ for each compartment

Compute $\mathbf{F}(\mathbf{X}^j, t_j) = [F_1, F_2, F_3, F_4, F_5, F_6, F_7, F_8]^\top$ using:

$$
\begin{aligned}
F_1 &= A_H - \frac{(b_1 + b_2) I_H^j S_H^j}{N_H} + v Q_H^j - m_H S_H^j \\
F_2 &= \frac{(b_1 + b_2) I_H^j S_H^j}{N_H} - (a_1 + a_2 + m_H) E_H^j \\
F_3 &= a_1 E_H^j - (m_H + d_H + r) I_H^j \\
F_4 &= a_2 E_H^j - (v + u + m_H + d_H) Q_H^j \\
F_5 &= r I_H^j + u Q_H^j - m_H R_H^j \\
F_6 &= A_R - \frac{b_3 S_R^j I_R^j}{N_R} - m_R S_R^j \\
F_7 &= \frac{b_3 S_R^j I_R^j}{N_R} - (a_3 + m_R) E_R^j \\
F_8 &= a_3 E_R^j - (d_R + m_R) I_R^j
\end{aligned}
$$

▷ Update solution using explicit κ-NFDM scheme from equation (23)

$$
\begin{aligned}
\mathbf{X}^{j+1} = \mathbf{X}^j &- \frac{1}{t_{j+1}^{1-\kappa}} \cdot \text{MemorySum} \\
&+ \frac{\theta(h) \cdot t_{j+1}^{\kappa-1} \cdot \Gamma(2-\lambda)}{\kappa^{\lambda-1}} \cdot \nu \cdot t_j^{\nu-1} \cdot \mathbf{F}(\mathbf{X}^j, t_j)
\end{aligned}
$$

▷ Ensure non-negativity (biological constraint)

$\mathbf{X}^{j+1} = \max(\mathbf{X}^{j+1}, \mathbf{0})$

▷ Store solution at crossover point

$\mathbf{X}_{t_1} = \mathbf{X}^{N_1}$

$t_{\text{current}} = t_1$

Step 3: Transition to Stochastic Regime

Set initial condition for stochastic part: $\mathbf{X}_{t_1}$ (from deterministic regime)

Generate fractional Brownian motion increments:

for $j = N_1 + 1$ to N **do**

  $\Delta B_j^{H^*} \sim \mathcal{N}(0, h^{2H^*})$ ▷ FBM increments with Hurst index H^*

end for

Step 4: Stochastic Regime - Nonstandard Modified Euler-Maruyama Method (NMEMM)

for $j = N_1$ to $N - 1$ **do**

  $t_{j+1} = t_{\text{current}} + h$

▷ Compute drift terms $\mathbf{F}(\mathbf{X}^j, t_j)$ (same as in Step 2)

Compute $\mathbf{F}(\mathbf{X}^j, t_j)$

▷ Apply NMEMM scheme from equation (24)

for $i = 1$ to 8 **do**

▷ Deterministic part with nonstandard denominator

DriftPart $= F_i(\mathbf{X}^j, t_j) \cdot \theta(h)$

▷ Stochastic part with FBM increment

DiffusionPart $= \sigma_i \cdot X_i^j \cdot \Delta B_j^{H^*}$

▷ Memory correction term for fractional Brownian motion

FBM_Correction $= 0.5 \cdot \sigma_i \cdot X_i^j \cdot \theta(h)^{2H^*}$

▷ Update i-th component

$X_i^{j+1} = X_i^j +$ DriftPart $+$ DiffusionPart $+$ FBM_Correction

end for

▷ Ensure non-negativity (biological constraint)

$\mathbf{X}^{j+1} = \max(\mathbf{X}^{j+1}, \mathbf{0})$

$t_{\text{current}} = t_{j+1}$

Step 5: Return Results

return $\mathbf{X}(t_j)$ for $j = 0, 1, 2, \ldots, N$

=0

6. Numerical Simulations

This section presents numerical simulations of the proposed stochastic fractal-fractional crossover model for monkeypox transmission (6-8), incorporating both deterministic and stochastic influences through Caputo-Katugampola derivatives and fractional Brownian motion. The simulations are conducted over two distinct time intervals, corresponding to the fractal-fractional deterministic regime and the stochastic regime, respectively. To validate the model's capacity to reproduce real epidemic patterns, we employ parameter values calibrated using real-world monkeypox outbreak data reported in the United States. The model is solved numerically using the κ-NFDM (23) (for the deterministic part) and NMEMM (24) (for the stochastic part), both of which are specifically adapted to the nonlocal memory structure of the system.

The parameter set employed in this study is as follows: $A_R = 0.60822$, $d_H = 0.015016$, $r = 0.067689$, $A_H = \frac{1}{79\times365}$, $a_3 = 0.025289$, $b_2 = 0.747322$, $b_1 = 0.011503$, $b_3 = 0.321102$, $a_1 = 0.423890$, $a_2 = 1.797575$, $v = 1.575454$, $u = 0.999763$, $m_H = \frac{1}{79\times365}$, $m_R = \frac{1}{5\times365}$, and $d_R = 0.000025$.

These parameters were determined through calibration with real-world monkeypox outbreak data reported in the United States, as referenced in [31]. The corresponding initial conditions for the system variables are provided below:
$\mathcal{Q}_{\mathcal{H}}(0) = 1.14$, $\mathcal{R}_{\mathcal{H}}(0) = 0$, $\mathcal{I}_{\mathcal{R}}(0) = 10$, $\mathcal{E}_{\mathcal{H}}(0) = 50$, $\mathcal{S}_{\mathcal{R}}(0) = 1000$, $\mathcal{I}_{\mathcal{H}}(0) = 5.86$, $\mathcal{S}_{\mathcal{H}}(0) = 10000$, and $T_f = 120$, $t_2 = 100$, and $t_1 = 40$, $\theta(h) = 1 - e^{-h}$, $t_{j+1} = (\varepsilon(j+1)h)$, ε is positive real number.We assess the performance of the proposed model by comparing the simulated number of infected human cases with actual outbreak data reported in the United States

during the period from June 13 to September 16, 2022, as shown in Figures 5–9. In these figures, we put $\varepsilon = 1$ and explore different scenarios by varying the fractional parameters ν, κ, H^*, and λ as follows:

Figure 5 show the simulation for $\lambda = 1$, $\nu = 0.98$, $\kappa = 0.98$, and $H^* = 0.90$.
This figure illustrates the model's behavior close to the classical derivative case ($\lambda = 1$), with mild fractal influence ($\nu < 1$) and memory captured via the Hurst index ($H^* = 0.90$). The infection trajectory aligns well with empirical data, indicating that small deviations from the classical model enhance realism while retaining interpretability. The result suggests that the inclusion of memory effects enables the model to better replicate the temporal characteristics of monkeypox outbreaks.

Figure 6 show the simulation for $\lambda = 0.99$, $\nu = 0.98$, $\kappa = 0.99$, and $H^* = 0.5$.
Here, the Hurst index $H^* = 0.5$ represents standard Brownian motion (no long-range dependence), while the fractional orders remain close to 1. This scenario shows increased fluctuation in the infection dynamics, emphasizing the role of memory in stabilizing trajectories. The figure underscores that stochastic noise alone cannot fully capture real-world epidemic trends without incorporating memory via fractional operators.

Figure 7 show the simulation for $\lambda = 0.97$, $\nu = 0.98$, $\kappa = 1$, and $H^* = 0.90$.
This case enhances memory effects in the fractional derivative while maintaining classical time scaling. The results show slower growth in infections, consistent with delayed epidemic progression. This biologically reflects situations where the population exhibits delayed transmission responses, extended incubation, or behavioral inertia—factors that commonly arise in real-world outbreaks.

Figures 8 and 9 show the simulation for $\lambda = 0.97$, $\nu = 1$, $\kappa = 0.97$, and $H^* = 0.90$.
These figures present simulations with pure fractional dynamics ($\nu = 1$) and sub-linear time scaling ($\kappa < 1$), coupled with strong memory effects. The infection curve is more gradual and reaches a lower peak, indicating reduced transmission acceleration. Biologically, this suggests that interventions (e.g., isolation, distancing) or inherent epidemiological features (e.g., long latency) are effectively slowing the epidemic.

The proposed model demonstrates strong predictive capability, yielding results that align more closely with observed data when compared to existing models in the literature, such as those presented in [40, 41]. Notably, our framework exhibits a significant improvement in performance.

Figure 10 illustrates the effect of varying the time-scaling parameter κ, while holding $\lambda = 0.98$, $\nu = 0.85$, and $H^* = 0.5$ fixed. This figure highlights how decreasing κ delays the onset of infection and smoothens the epidemic trajectory. Biologically, this behavior aligns with phenomena such as delayed diagnosis, underreporting, or lag in public health responses. These findings emphasize the critical role of time-scaling in shaping the timing and intensity of outbreaks.

Figure 11 explores the influence of the fractional and fractal orders, λ and ν, respectively, under fixed values of $\kappa = 0.98$ and $H^* = 0.90$. The simulation reveals that lower values of these parameters are associated with prolonged, slower infection dynamics. This reflects memory-driven epidemiological effects, including delayed disease progression, behavioral adaptation, and immune memory. Such results underscore the model's capacity to represent nuanced temporal patterns observed in real-world monkeypox epidemics.

Overall, our model clearly outperforms conventional integer-order and classical fractional

models discussed in prior studies [31, 40].

Overall, the simulations emphasize that a fractional-stochastic modeling framework is more suitable than classical approaches for capturing the nuanced and persistent nature of monkeypox transmission. The biological interpretation underscores the need to account for memory, stochasticity, and scale effects in designing robust and timely control strategies.

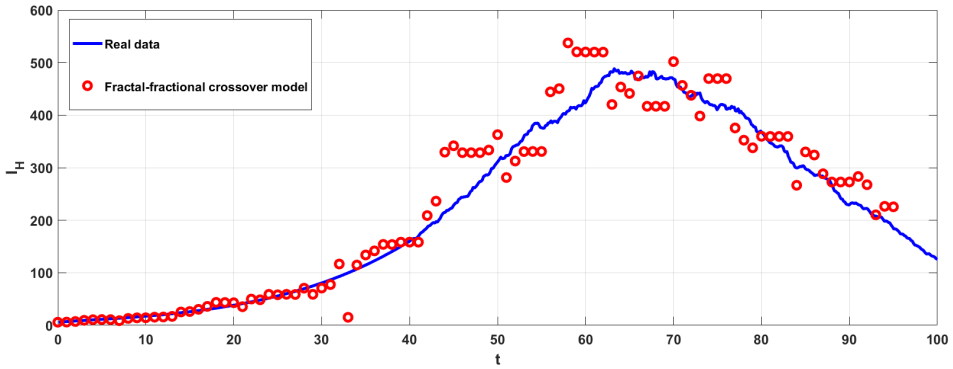

Figure 5: Simulation for (6-8), and $\lambda = 1, \nu = 0.98,\ H^* = 0.90,\ \kappa = 0.98,\ \sigma_1 = 0.05, \sigma_2 = 0.02, \sigma_3 = 0.02, \sigma_4 = 0.05, \sigma_5 = 0.02, \sigma_6 = 0.02, \sigma_7 = 0.05, \sigma_8 = 0.02.$

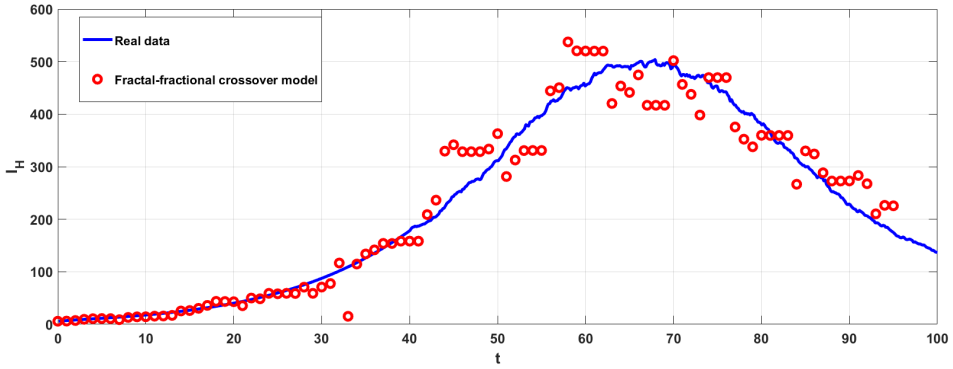

Figure 6: Simulation for (6-8), and $\lambda = 0.99, \nu = 0.98,\ H^* = 0.5,\ \kappa = 0.99,\ \sigma_1 = 0.05, \sigma_2 = 0.02, \sigma_3 = 0.02, \sigma_4 = 0.05, \sigma_5 = 0.02, \sigma_6 = 0.02, \sigma_7 = 0.05, \sigma_8 = 0.02.$

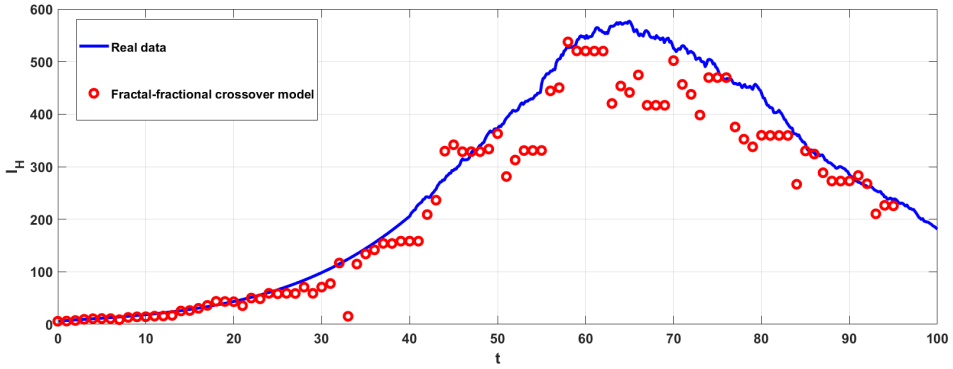

Figure 7: Simulation for (6-8), and $\lambda = 0.97$, $\nu = 0.98$, $H^* = 0.9$, $\kappa = 1$, $\sigma_1 = 0.05$, $\sigma_2 = 0.02$, $\sigma_3 = 0.02$, $\sigma_4 = 0.05$, $\sigma_5 = 0.02$, $\sigma_6 = 0.02$, $\sigma_7 = 0.05$, $\sigma_8 = 0.02$,

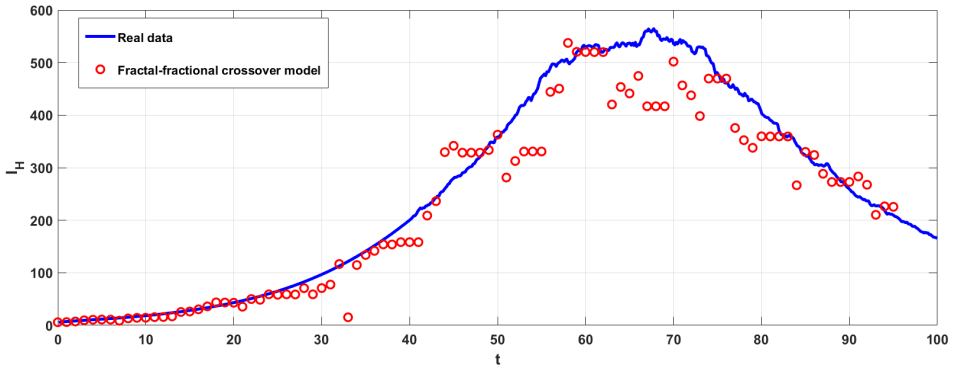

Figure 8: Simulation for (6-8), and $\lambda = 0.97$, $\nu = 1$, $H^* = 0.90$, $\kappa = 0.97$, $\sigma_1 = 0.05$, $\sigma_2 = 0.02$, $\sigma_3 = 0.02$, $\sigma_4 = 0.05$, $\sigma_5 = 0.02$, $\sigma_6 = 0.02$, $\sigma_7 = 0.05$, $\sigma_8 = 0.02$.

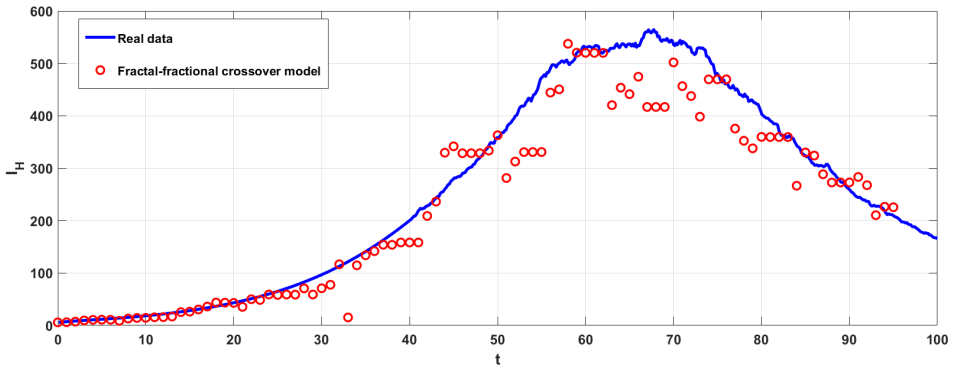

Figure 9: Simulation for (6-8), and $\lambda = 0.97$, $\nu = 1$, $H^* = 0.90$, $\kappa = 0.97$, $\sigma_1 = 0.05$, $\sigma_2 = 0.02$, $\sigma_3 = 0.02$, $\sigma_4 = 0.05$, $\sigma_5 = 0.02$, $\sigma_6 = 0.02$, $\sigma_7 = 0.05$, $\sigma_8 = 0.02$.

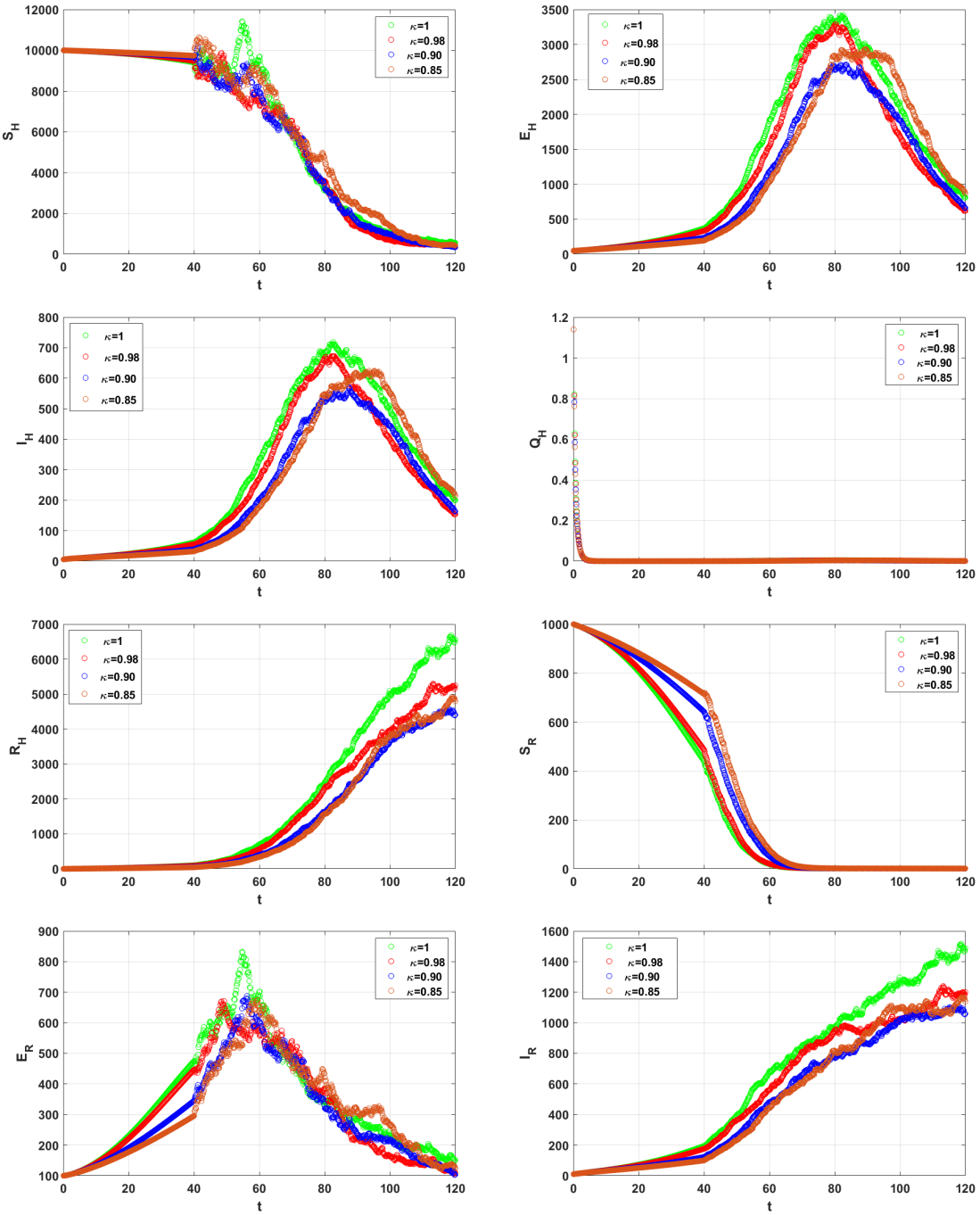

Figure 10: Simulation for (6-8) and different value of κ with $\lambda = 0.98$, $\nu = 0.85$, and $H^* = 0.5$, $\sigma_1 = 0.05$, $\sigma_2 = 0.02$, $\sigma_3 = 0.02$, $\sigma_4 = 0.05$, $\sigma_5 = 0.02$, $\sigma_6 = 0.01$, $\sigma_7 = 0.05$, $\sigma_8 = 0.02$.

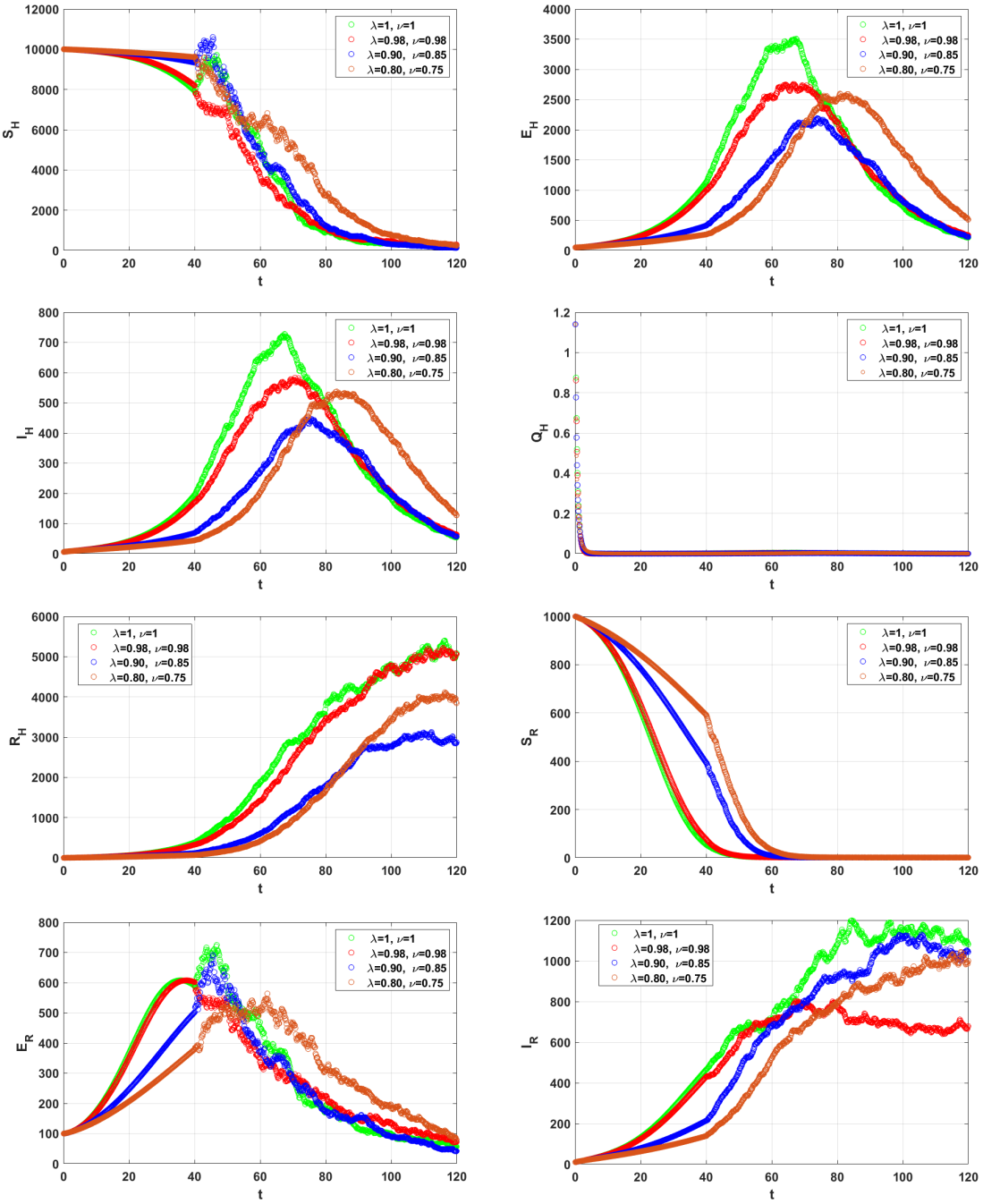

Figure 11: Simulation for (6-8) and different value of λ, ν, with $\kappa = 0.98$, and $H^* = 0.90$, $\sigma_1 = 0.05$, $\sigma_2 = 0.02$, $\sigma_3 = 0.02$, $\sigma_4 = 0.05$, $\sigma_5 = 0.02$, $\sigma_6 = 0.01$, $\sigma_7 = 0.05$, $\sigma_8 = 0.02$.

7. Conclusions

In this study, we developed a novel crossover model for monkeypox transmission dynamics based on a hybrid framework that combines fractal-fractional Caputo-Katugampola derivatives with stochastic perturbations driven by fractional Brownian motion. The model captures both deterministic memory effects and random environmental fluctuations by employing a piecewise formulation across two time intervals, reflecting realistic transitions in disease progression and control response.

We established the existence and uniqueness of solutions using generalized Banach space theory and the Perov fixed point theorem, ensuring the model's mathematical well-posedness. To obtain numerical solutions, we constructed a κ-nonstandard finite difference method for the deterministic regime and a nonstandard modified Euler-Maruyama scheme for the stochastic regime, both adapted to the fractional and fractal nature of the system.

Sensitivity analysis identified b_2 and b_1 as the most influential parameters affecting the number of infected individuals. Bifurcation analysis revealed a forward (supercritical) bifurcation, indicating a smooth transition from disease-free to endemic states as transmission rates increase. Numerical simulations, supported by real data from the United States, confirmed the model's ability to reproduce observed outbreak patterns and demonstrated the significant impact of fractional orders, time-scaling, and memory on infection dynamics.

Overall, this work illustrates the power of combining fractal-fractional calculus with stochastic modeling to better understand and predict the spread of emerging zoonotic diseases such as monkeypox. The proposed model outperforms classical and conventional fractional models, providing a more accurate and flexible framework for forecasting and control. Limitations include homogeneous mixing assumptions, absence of spatial heterogeneity, and computational costs of FBM simulations. Future work will incorporate spatial structure, time-dependent parameters, optimal control strategies, and applications to other emerging zoonotic diseases.

Acknowledgements

The authors T.Abdeljawad and H. M. Alkhawar would like to thank Prince Sultan University for paying the APC and for the support through the TAS research lab.

Data Availability Statement: The data that support the findings of this study are available from the corresponding author upon reasonable request.

Conflicts of Interest: The authors declare no conflicts of interest.

References

[1] Centers for Disease Control and Prevention (CDC). About mpox, 2024. Updated April 18, 2024.

[2] World Health Organization. Mpox (monkeypox), 2023. Accessed 11 Dec 2023.

[3] World Health Organization. Who recommends new name for monkeypox disease, 2022. Accessed 28 Nov 2022.

[4] World Health Organization. Mpox (monkeypox) outbreak 2022 – global, 2024. Accessed May 21, 2024.

[5] H. W. Hethcote. The mathematics of infectious diseases. *SIAM Review*, 42(4):599–653, 2000.

[6] R. L. Magin. *Fractional Calculus in Bioengineering*. Begell House Publishers, 2006.

[7] K. Diethelm. Predicting the dynamics of epidemics using fractional calculus. *Nonlinear Dynamics, Psychology, and Life Sciences*, 12(3):251–261, 2008.

[8] A. Atangana and D. Baleanu. A new fractional derivative with non-local and non-singular kernel: theory and application to heat transfer model. *Thermal Science*, 20(2):763–769, 2018.

[9] A. Atangana and S. İ. Araz. New concept in calculus: Piecewise differential and integral operators. *Chaos, Solitons & Fractals*, 145:110638, 2021.

[10] A. Atangana and I. Koca. Modeling the spread of tuberculosis with piecewise differential operators, 2021. Preprint.

[11] F. Alalhareth, S. M. Al-Mekhlafi, A. Boudaoui, N. Laksaci, and M. H. Alharbi. Numerical treatment for a novel crossover mathematical model of the covid-19 epidemic. *AIMS Mathematics*, 9(3):5376–5393, 2024.

[12] A. Atangana and S. İ. Araz. Modeling third waves of covid-19 spread with piecewise differential and integral operators: Turkey, spain and czechia. *Results in Physics*, 29:104694, 2021.

[13] N. H. S weilam, S. M. Al-Mekhlafi, S. M. Hassan, N. R. Alsenaideh, and A. E. Radwan. A novel hybrid crossover dynamics of monkeypox disease mathematical model with time delay: Numerical treatments. *Fractal and Fractional*, 8(4):185, 2024.

[14] K. Shah, H. Naz, T. Abdeljawad, and B. Abdalla. Study of fractional order dynamical system of viral infection disease under piecewise derivative. *CMES-Computer Modeling in Engineering & Sciences*, 136(1), 2023.

[15] W. Kumlachew. Modelling the impact of sexual activities and inflow of sexually active infected immigrants on hiv/aids epidemics. *Journal of Mathematical Analysis and Modeling*, 3(3), 2022.

[16] F. A. Rihan, U. Kandasamy, H. J. Alsakaji, and N. Sottocornola. Dynamics of a fractional-order delayed model of covid-19 with vaccination efficacy. *Vaccines*, 11(4):758, 2023.

[17] R. Chinnathambi, F. A. Rihan, and H. J. Alsakaji. A fractional-order model with time delay for tuberculosis with endogenous reactivation and exogenous reinfections. *Mathematical Methods in the Applied Sciences*, 44:8011–8025, 2021.

[18] M. M. Abou Hasan. An efficient discretization scheme for a time-delay variable-order fractional diabetes model. *Mathematical Methods in the Applied Sciences*, 49(2):960–976, 2025.

[19] M. M. Abou Hasan, A. M. Alghanmi, S. M. Al-Mekhlafi, H. Al Ali, and Z. Mukandavire. A novel crossover dynamics of variable-order fractal-fractional stochastic diabetes model: Numerical simulations. *Journal of Mathematics*, pages 1–22, 2025.

[20] S. M. Al-Mekhlafi, M. M. Abou Hasan, H. A. Al-Ali, and Z. Mukandavire. A crossover optimal control framework for a time-delayed fractional-order diabetes model: Stability, bifurcation, and numerical analysis. *Mathematical Methods in the Applied Sciences*, 48(17):15723–15741, 2025.

[21] S. M. Al-Mekhlafi. Efficient numerical method for solving a cancer tumor model governed by fractional partial differential equations involving the ψ-caputo derivative. *Sana'a University Journal of Applied Sciences and Technology*, 4(2):1682–1693, 2026.

[22] S. M. Al-Mekhlafi, K. R. Raslan, K. K. Ali, S. H. Alssad, and N. R. Alsenaideh. Numerical treatments for a crossover cholera mathematical model combining different fractional derivatives based on nonsingular and singular kernels. *Computer Modeling in Engineering & Sciences*, 143(2), 2025.

[23] S. M. Al-Mekhlafi. A novel crossover variable order (deterministic-stochastic) lung cancer and tumor-immune system interaction: Numerical simulations. *Progress in Fractional Differentiation and Applications*, 11(1):73–86, 2025.

[24] U. N. Katugampola. New approach to a generalized fractional integral. *Applied Mathematics and Computation*, 218:860–865, 2011.

[25] U. N. Katugampola. A new approach to generalized fractional derivative. *Bulletin of Mathematical Analysis and Applications*, 6(4):1–15, 2014.

[26] U. N. Katugampola. Existence and uniqueness results for a class of generalized fractional differential equations, 2014. arXiv:1411.5229, preprint.

[27] A. Atangana and S. Qureshi. Modeling attractors of chaotic dynamical systems with fractal-fractional operators. *Chaos, Solitons and Fractals*, 123:320–337, 2019.

[28] N. H. S weilam, S. M. Al-Mekhlafi, and D. G. Mohamed. Novel chaotic systems with fractional differential operators: Numerical approaches. *Chaos, Solitons and Fractals*, 2020.

[29] A. A. Kilbas, H. H. Srivastava, and J. J. Trujillo. *Theory and Applications of Fractional Differential Equations*. Elsevier, Amsterdam, 2006.

[30] A. M. Shloof, N. Senu, A. Ahmadian, and S. Salahshour. An efficient operation matrix method for solving fractal–fractional differential equations with generalized caputo-type fractional–fractal derivative. *Mathematics and Computers in Simulation*, 188:415–435, 2021.

[31] O. J. Peter, S. Kumar, N. Kumari, F. A. Oguntolu, K. Oshinubi, and R. Musa. Transmission dynamics of monkeypox virus: a mathematical modelling approach. *Modeling Earth Systems and Environment*, 8(3):3423–3434, 2022.

[32] J. F. Gómez-Aguilar, J. J. Rosales-García, J. J. Bernal-Alvarado, T. Córdova-Fraga, and R. Guzmàn-Cabrera. Fractional mechanical oscillators. *Revista Mexicana de Física*, 58:348–352, 2012.

[33] M. Z. Ullah and D. Baleanu. A new fractional sica model and numerical method for the transmission of hiv/aids. *Mathematical Methods in the Applied Sciences*, pages 1–12, 2021.

[34] A. Perov. On the cauchy problem for a system of ordinary differential equations. *Pviblizhen. Met. Reshen. Differ. Uvavn*, 2:115–134, 1964.

[35] D. Nualart and A. Răşcanu. Differential equations driven by fractional brownian motion. *Collectanea Mathematica*, 53(1):55–81, 2002.

[36] Y. Hu and D. Nualart. A differential equation driven by fractional brownian motion. *Stochastic Analysis and Applications*, 28(5):796–817, 2010.

[37] S. Zeng, D. Baleanu, Y. Bai, and G. Wu. Fractional differential equations of caputo-katugampola type and numerical solutions. *Applied Mathematics and Computation*, 315:549–554, 2017.

[38] R. E. Mickens. *Nonstandard Finite Difference Models of Differential Equations*. World Scientific, Singapore, 2005.

[39] Y. Hu, Y. Liu, and D. Nualart. Modified euler approximation scheme for stochastic differential equations driven by fractional brownian motions, 2013. arXiv:1306.1458v1 [math.PR].

[40] P. Kumar, M. Vellappandi, Z. Khan, S. M. Sivalingam, A. Kaziboni, and V. Govindaraj. A case study of monkeypox disease in the united states using mathematical modeling with real data. *Mathematics and Computers in Simulation*, 213:444–465, 2023.

[41] N. H. S weilam, S. M. Al-Mekhlafi, S. M. Hassan, N. R. Alsunaideh, and A. E. Radwan. A novel hybrid crossover dynamics of monkeypox disease mathematical model with time delay: Numerical treatments. *Fractal and Fractional*, 8(4):185, 2024.